Lawrence Berkeley National Laboratory

Title
THE ROLE OF THE MICROSTRUCTURAL COMPONENTS IN A THREE-STEP HEAT CYCLED, LOW CARBON Fe-6Ni ALLOY

Permalink
https://escholarship.org/uc/item/6k0157t7

Author
Kim, H.J.

Publication Date
1981-05-01

Lawrence Berkeley Laboratory

UNIVERSITY OF CALIFORNIA

Materials & Molecular Research Division

THE ROLE OF THE MICROSTRUCTURAL COMPONENTS IN A
THREE-STEP HEAT CYCLED, LOW CARBON Fe-6Ni ALLOY
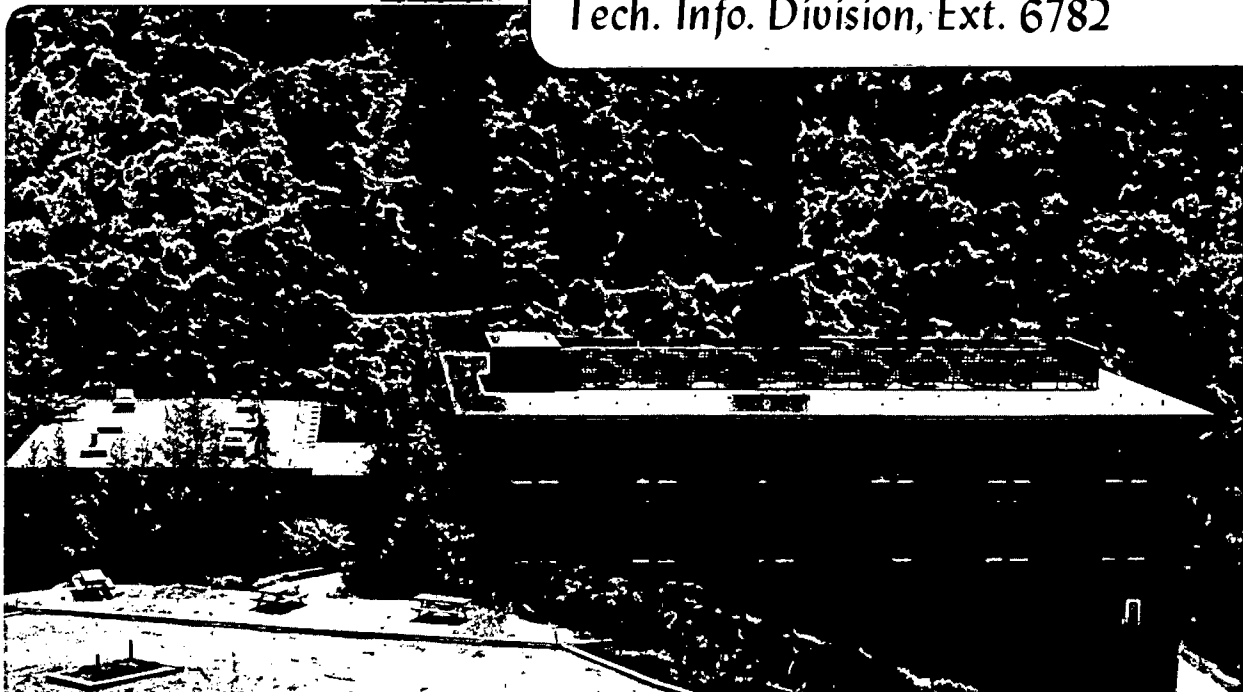
Hee Jae Kim
(M.S. thesis)

May 1981

DISCLAIMER

THE ROLE OF THE MICROSTRUCTURAL COMPONENTS IN A

THREE-STEP HEAT CYCLED, LOW CARBON Fe-6Ni ALLOY

Hee Jae Kim

M.S. Thesis

May 1981

Materials and Molecular Research Division
Lawrence Berkeley Laboratory
University of California
Berkeley, CA 94720
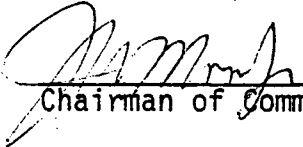
THE ROLE OF THE MICROSTRUCTURAL COMPONENTS IN A

THREE-STEP HEAT CYCLED, LOW CARBON Fe-6Ni ALLOY

Master of Science   Hee Jae Kim   Physical Metallurgy
of Engineering

Chairman of Committee

ABSTRACT

The role of each microstructural component (i.e., ultrafine-grain, stable retained austenite, and tempered martensite matrix) in a three-step heat cycled, low carbon Fe-6Ni cryogenic alloy, which had shown excellent cryogenic properties, were studied independently through investigations of the mechanical properties and transformational behaviors of two simulated alloys. As a result, it was found that each component contributed to overall properties of the cryogenic alloy uniquely as follows: (1) The ductile-brittle transition temperature is suppressed effectively by grain refinement. (2) Stable retained austenite in ferritic steel increases the cryogenic toughness by grain refinement. (3) The martensite matrix of ferritic steel affects the Charpy upper shelf energy alone. It also was found that an excellent cryogenic toughness was obtainable by the combined effects of each microstructural component of the alloy.

ACKNOWLEDGEMENTS

The author wishes to express his deep gratitude to Professor J. W. Morris, Jr. for his guidance and encouragement during the course of this investigation. He is also grateful to Professor D. P. Whittle and Professor M. F. Merriam for their review of this manuscript. Thanks are also due to Drs. Chol K. Syn and Jungihl Kim for their advice and encouragement.

The author is gratefully indebted to his country, Korea, and to his family, especially his parents and his dear fiancee, Hee-Sook, for their encouragement.

iii

TABLE OF CONTENTS

I. INTRODUCTION

The increase in structural applications of steel for use in liquefied natural gas and other lower temperatures has generated a need for cryogenic alloys of high strength and toughness. Austenitic stainless steels, Invar alloys, and 9Ni steel[1,2] were commonly specified for these applications. However, because of economic considerations, 5Ni[3] and 6Ni steel[4-6] were recently introduced in the United States and Japan with excellent cryogenic properties comparable to 9Ni steel.

These ferritic (5-9)Ni cryogenic steels which are intended for structural use at cryogenic temperatures are usually given an intercritical tempering in the two-phase ($\alpha + \gamma$) region of the phase diagram which introduces a fine stable precipitated austenite in a grain-refined tempered martensite (or ferrite) matrix.[1,4-10] The intercritical tempering lowers the ductile-brittle transition temperature of the alloy to below liquid nitrogen temperature.[6,7,11] This has been generally believed due to the retention of a small fraction of precipitated austenite in the ferritic matrix[5,6,10,12] and fine grain size.[12-14] Numerous investigations have presented plausible explanations for how the retained austenite and grain size contribute to the cryogenic toughness.[5-7,10,12-16] However, there has been inconsistent reporting of the quantitative and qualitative effect of retained austenite depending upon the alloy investigated.[9,10,13-16] Such discrepancies in the effect of retained austenite phase have raised a doubt whether the excellent cryogenic toughness of ferritic cryogenic steels comes[5] from the retained austenite phase itself as reported previously[1,4,7,17-19] or from the combined effect of each microstructural component (i.e., ultrafine-grain, stable retained austenite, and tempered martensite matrix). Such a doubt is

reasonable if it is taken into account that tempered martensite is the main component of the cryogenic ferritic steel final microstructure (around 90 pct) and that its effects have so far been largely ignored. Moreover, if the combined microstructural components lead to an excellent cryogenic toughness, they bring up a new question about the individual role of each component on the properties. Clarifying this point is important to guide the direction of further research in alloy design as well as basic research itself.

The present research was undertaken to characterize the final microstructures which show excellent cryogenic properties and to clarify the individual effect of retained austenite, ferrite matrix, and grain size. In order to achieve these purposes, the following approach was taken: First, two alloys were prepared having compositions close to those of the retained austenite and ferrite matrix of the base 6Ni cryogenic steel in its heat treated condition. Second, the alloys were given the conventional heat treatment for 6Ni cryogenic steel. Third, the mechanical properties and transformational behavior of the two alloys were investigated. Fourth, the properties of the alloys were compared with those of the base alloy.

A commercial low carbon Fe-6Ni alloy was adopted as the base alloy for this research since the alloy in the so-called QLT treatment has a microstructure of grain-refined tempered martensite (or ferrite) matrix with a stable retained austenite showing successful depression of the ductile-brittle transition temperature to below liquid nitrogen temperature.[5,10,12,15,16] The commercial QLT heat treatment employed for the Fe-6Ni alloy is austenitizing (Q) at 800°C, intercritical annealing (L) at relatively high temperature (670°C) in the two-phase (α + γ) region to achieve a grain refining, and intercritical tempering (T) at relatively low temperature (600°C) in the two-phase (α + γ) region to introduce a slight admixture of thermally

stable austenite phase. In an earlier work in this laboratory,[20] the chemical compositions of the retained austenite and tempered martensite matrix of the QLT-treated Fe-6Ni base alloy were determined by scanning transmission electron microscopic analysis. Based on this result, two alloys which had similar chemical compositions to those of the retained austenite and those of tempered martensite matrix in the Fe-6Ni base alloy were made. Mechanical properties and transformational behavior of the simulated alloys were investigated separately and compared with those of the base alloy in order to determine the net effect of each component.

II. EXPERIMENTAL PROCEDURE

A. Material Preparation and Heat Treatments.

1. Base Alloy.

Commercial low carbon Fe-6Ni alloy and Fe-9Ni alloy were provided by the Nippon Steel Corp. and by Nippon Kokan K.K., respectively. The as-received alloys were annealed at 1200°C for 2 hours to remove the effects of prior deformation and heat treatments. The alloys were then solution-annealed at 900°C for 2 hours before heat treatment. The chemical composition of the commercial alloy is given in Table I. The heat treatment of this Fe-6Ni alloy was the three-step, QLT treatment,[6,20] where Q is an austenitizing treatment at 800°C for 1 hour, L is an intercritical annealing in the two-phase ($\alpha+\gamma$) region at 670°C for 1 hour, and T is an intercritical tempering in the two-phase ($\alpha+\gamma$) region at 600°C for 1 hour.

2. Alloy M and Alloy A.

Two alloys of nominal compositions Fe-5Ni and Fe-9Ni-3Mn were made by induction melting in an argon gas atmosphere. The Fe-5Ni alloy represents the matrix and Fe-9Ni-3Mn alloy represents the retained austenite phase in the QLT-treated Fe-6Ni base alloy. The chemical compositions of the alloys were determined from a previous scanning transmission electron microscopy analysis[20] of the composition of retained austenite and tempered martensite matrix in the Fe-6Ni base alloy. The analyzed chemical compositions of the two phases in the base alloy are presented in Table I. However, since the carbon content in the two phases had not been determined in the previous research,[20] it was theoretically determined as follows: the tempered martensite (or ferrite) matrix is assumed to have a carbon content equal to the maximum solubility in ferrite at the final tempering temperature (i.e., ~0.01 pct at 600°C) and the retained austenite was assumed to contain the

rest of the carbon. Since the volume fraction of the reverted austenite after 1 hour tempering at 600°C was approximately 10 pct,[20] the average carbon content in the retained austenite can be determined as ((carbon pct in the base alloy)-(maximum solubility of carbon in ferrite matrix at final tempering temperature) x (volume fraction of ferrite))/(volume fraction of the retained austenite) and is about 0.5 pct. Other interstitial elements in the retained austenite were ignored. The chemical composition of the simulated Fe-5Ni alloy (denoted by alloy M below) and Fe-9Ni-3Mn alloy (denoted by alloy A below) are also presented in Table I.

The simulated alloys M and A were homogenized under an argon gas atmosphere at 1200°C for 28 hours, and then air-cooled to room temperature. They were forged at approximately 1100°C in a single heat into plates of dimensions of 22.9 mm (0.9 in.) x 76.2 mm (3.0 in.) cross-section. Mechanical property test specimens were cut from the plate. The specimens were solution-annealed at 900°C for 2 hours and water-quenched to room temperature before final heat treatment. The transformation temperatures of the alloy M were investigated by dilatometry to decide the heat treatment temperature. They are presented in Table II. Alloy M was heat-treated basically by the three-step, QLT thermal cycling as had been the Fe-6Ni base alloy. An intercritical annealing temperature of 710°C was used for this alloy since the austenite transformation temperatures (A_s and A_f temperature) of alloy M are about 50°C higher than those of the base alloy. The alloy M in an as-quenched condition (Q) and as-quenched and tempered condition (QT) were also studied. To investigate the net effect of grain size, the solution-annealed alloy M was thermomechanically treated, that is, cold-worked by 25 pct or 50 pct followed by the QLT heat treatment. For alloy A only solution-annealed treatment at 800°C for 1 hour was used since no phase transformation was found

during quenching down to room temperature. The solution-annealed alloy A was also cold-worked by 30 pct and then solution-annealed again for grain refinement. The alloys investigated in the present research were water-quenched to room temperature after each heat treatment.

In order to investigate the effect of matrix alone, up-quenching treatments as designated in Fig. 1, which is a fast heating to 850°C in an induction furnace and immediately quenching into ice brine, was applied to the QLT-treated Fe-6Ni base alloy, QT-treated alloy M, and QT-treated commercial Fe-9Ni alloy. This heat treatment was conducted within around 12 seconds and intended to obtain a different state of matrix structure minimizing a change in grain size.

B. Dilatometry Measurement.

Standard dilatometry test specimens (Fig. 2) for use in a Theta Dilatronic III R dilatometer were machined from bulk material and tested to measure the phase transformation temperatures. A programmed linear heating and cooling rate of 45°C/min. was used. The first deviation point from linearity on dilation in a temperature versus time chart was taken as transformation temperature.

C. Mechanical Testing.

1. Tensile Testing.

Cylindrical compact tensile specimens (Fig. 3) were machined from the heat-treated blanks. The rolling direction of the plate was parallel to the axial loading direction of the specimens. Tensile tests were conducted at room temperature and a liquid nitrogen temperature (-196°C) on an Instron testing machine employing a strain rate of 0.127 cm/min. (0.05 in./min.).

The yield strength was calculated by the 0.2 pct offset method. Total elongation and reduction in area were measured in a travelling microscope with an accuracy of ± 0.01 mm. Three specimens were tested for each data point.

2. Charpy Impact Testing.

Charpy V-notch impact specimens of ASTM standard size (Fig. 4) were machined along the rolling directions of the plates. The Charpy impact tests were conducted as described in ASTM E 23-72. Testing temperatures were controlled by a proper mixture of liquid nitrogen and isopentane.

D. X-ray Diffraction Analysis.

X-ray diffraction analyses were used to identify the austenite phase and to determine the volume fraction of retained austenite. In order to eliminate an error due to mechanically-induced transformation of retained austenite on the cut surfaces, specimens were polished and chemically thinned in a solution of 100 ml H_2O_2 + 3 ml HF for 30 minutes. After these treatments, the specimens were scanned with a Picker x-ray diffractometer using Fe K_α radiation. The calculation of the volume fraction of retained austenite was based on Miller's method[21] comparing the x-ray integrated intensities of $(211)_\alpha$ with the mean values of the integrated intensities of $(220)_\gamma$ and $(311)_\gamma$.

E. Microscopy.

1. Optical Microscopy.

Specimens for optical microscopic studies were cut from broken Charpy bars and then mounted in Bakelite using a Struers hot press. After grinding, polishing was performed on 1 μm diamond past lapping wheel using kerosene as a lubricant. The specimens were then etched with 5 pct nital solution and all micrographs were taken in a Zeiss metallograph.

2. Scanning Electron Microscopy.

Fracture surfaces of the broken Charpy specimens were examined in an AMR-1000 scanning electron microscope with secondary emission at 20 KV.

3. Transmission Electron Microscopy.

Thin foils of about 0.305 mm (12 mils) thick were cut from borken Charpy specimens. These foils were chemically thinned to about 0.127 mm (5 mils), using a solution of 100 ml H_2O_2 + 3 ml HF, spark cut to 3 mm discs, and ground down to approximately 0.05 mm (2 mils) in thickness. These thin foils were jet polished at room temperature using a solution of 400 ml CH_3COOH + 75 g CrO_3 + 21 ml H_2O at approximately 40 Volts. These thin foils were examined in JEM 7A electron microscope using 100 KV acclerating voltages.

III. RESULTS

A. Effect of Grain Size.

Alloy M was used to study the effects of grain size only since no retained austenite phase was detected at room temperature after any of the thermal treatments used for this alloy. Different grain sizes were obtained in the alloy M by employing a controlled amount of cold work, then solution-annealing the alloy, after which the three-step, QLT heat treatment was applied. These thermomechanical treatments were selected because they were able to reduce the grain size very effectively[22] and also were able to control the grain size by the amount of cold working as shown in previous research.[23] The microstructures obtained after thermomechanical treatment are illustrated by the optical micrographs presented in Fig. 5. All microstructures consisted of tempered martensite. X-ray diffractometric test showed no indication of the presence of retained austenite phase in alloy M. As shown in Fig. 5, the grain size was changed from ~10 μm to ~5 μm and ~2 μm by introducing 25 pct and 50 pct cold working, respectively. It is evident that alloy M has been microstructurally refined by the cold working prior to heat treatment.

The Charpy impact energy of the alloy M is plotted as a function of the test temperature in Fig. 6. Interesting phenomena are observed in the effect of grain size. The upper shelf energy of Charpy impact is not affected by grain refinement. However, the ductile-brittle transition temperature is suppressed by refining the grain size. In this research, the transition temperature was decreased from -130°C to -150°C and -170°C by 25 pct and 50 pct cold working, respectively. These decreases in the transition temperature are believed to be totally due to the grain refinement since all microstructures of the specimens in Fig. 5 are tempered martensite without any

presence of retained austenite.

The results of tensile tests on the cold-worked alloy M at room temperature are presented in Table III. They show a slight increase in yield strength upon grain refinement. The ultimate tensile strength, on the other hand, is relatively unaffected by grain refinement. The total elongation and reduction in area also is not affected by grain refinement taking into account possible errors during test. This observation is consistent with Miller's result.[22] He showed that the reduction in area of 9Ni steel was essentially unchanged over a wide ultrafine-grain range.

B. Effect of Retained Austenite.

Alloy A which had a chemical composition similar to that of the retained austenite phase in the Fe-6Ni base alloy was used to characterize the net effect of retained austenite on the mechanical properties of ferritic cryogenic steel. Microstructures of alloy A were investigated by optical microscopy, transmission electron microscopy, and x-ray diffractometry. Optical micrographs illustrated in Figs. 7(a) and 8(a) show the microstructures obtained after the solution annealing treatment. X-ray diffraction revealed that those microstructures were totally austenite phase at room temperature. Transmission electron microscopic study of the microstructure of alloy A is presented in Fig. 9. It shows a complete austenitic phase, in agreement with optical microscopy and x-ray diffraction.

In order to investigate the thermal stability of the austenite, alloy A was quenched to liquid nitorgen temperature (-196°C) and liquid helium temperature (-269°C), respectively. Figure 7(b) shows the optical micrograph of alloy A after quenching to liquid nitrogen temperature. Figure 8(b) shows the optical micrograph of alloy A after quenching to liquid helium

temperature. Both optical micrographs illustrate that alloy A treated by
liquid nitrogen and liquid helium was somewhat transformed to martensite.
X-ray diffraction revealed that about 25 pct and 56 pct of the alloy trans-
formed to a mixture of lath martensite and plate martensite structure by
quenching to -196°C and -269°C, respectively. Annealing twins were ob-
served sometimes on the well-known (11̄1) twin plane as shown in Fig. 10
and many carbide precipitates were also found at austenite grain boundaries
as shown in Fig. 11.

However, the thermally stable austenitic alloy A was found to be very
susceptible to transformation on strain. Figure 12 shows the cross-section
of a Charpy impact test specimen broken at room temperature. Strain-induced
martensite appeared in a region as deep as 1,000 μm (1 mm) below the broken
fracture surface.

The transformation behavior of the alloy A, which is thermally stable but
mechanically unstable, is quite consistent with that of the retained austenite
in Fe-6Ni base alloy[20] and commercial Fe-9Ni alloy.[19]

Table IV lists the mechanical properties of the alloy A. As shown in
Table IV, the Charpy V-notch impact energy was not high either at room tem-
perature or at liquid nitrogen temperature. A brittle, quasi-cleavage
fracture mode appeared in the scanning electron fractographs at both tem-
peratures as shown in Figs. 13 and 14. The Charpy impact energy of the
alloy A turned out to be very small at both room temperature and liquid
nitrogen temperature when compared with that of the Fe-6Ni base alloy. This
comparison seems to indicate that retained austenite is not a source of high
impact toughness of the base alloy. However, as seen in most austenitic
alloys, the alloy A did not show any sudden transition to brittle fracture
with decreasing test temperature.

As shown in Table IV, the yield strength and reduction in the area of Alloy A are low when compared with those of the Fe-6Ni base alloy. This discrepancy seems to be due to the fact that a continuous transformation to martensite phase during the tensile test enhanced its work hardening,[24] while at the same time inhibiting necking of the specimen.

In order to investigate the effect of grain size in alloy A, the alloy was cold-worked by 30 pct and then solution-annealed. This treatment reduced the grain size of alloy A. However, the Charpy impact energy at both room temperature and liquid nitrogen temperature was not changed by the grain refinement of alloy A. This result is quite consistent with that of alloy M as described previously such that the grain refinement does not affect the shelf energy.

C. Effect of Tempered Martensite Matrix.

Alloy M was heat treated in four ways: as-quenched (Q), as-quenched and tempered (QT), basic three-step, QLT treated, and three-step, QL'T treated condition (L' treatment means that the intercritical annealing is done at 710°C as described previously.). The microstructures obtained after these heat treatments are shown by optical micrographs presented in Fig. 15. As shown in Fig. 15, the grain sizes of these specimens was considerably larger than that of the Fe-6Ni base alloy after identical heat treatments. This seems due to a lower carbon content in the alloy M. Karlsson[25] has shown that reducing the grain size is much easier with relatively higher carbon content level for the same heat treatment. Fig. 16 shows the transmission electron micrographs of these four heat treatments. The structure of the as-quenched alloy M is lath martensite, while those of alloy M with the other heat treatments are tempered martensite. X-ray diffraction and

transmission electron microscopy revealed that austenite phase did not exist in the alloy M regardless of heat treatment.

Table V illustrates the mechanical properties of alloy M after different heat treatments. As shown in this table, none of those heat treatments resulted in a reasonably high impact toughness at liquid nitrogen temperature. All mechanical properties of the QLT-treated alloy M except the Charpy impact energy at liquid nitrogen temperature are almost the same as those of the QL'T-treated alloy. However, the yield and ultimate tensile strengths were slightly decreased by adding an additional thermal treatment step while the total elongation and reduction in area were slightly increased. This appeared to be due to the reduced dislocation density after an intercritical annealing and tempering. Table V also reveals that the total elongation for alloy M at liquid nitrogen temperature is higher than that for room temperature even though the reduction in area of the alloy is decreased.

As shown in Table V, the Charpy impact energy of alloy M was very small at liquid nitrogen temperature. As described previously, even though grain refinement of alloy M suppressed the transition temperature very effectively, comparable impact toughness to that of Fe-6Ni base alloy at liquid nitrogen temperature was not obtained in alloy M. Scanning electron fractographs taken from the fracture surfaces of the alloy as shown in Figs. 17 and 18, showed tear fracture modes for room temperature, but complete brittle cleavage fracture modes for liquid nitrogen temperature.

In order to study what kind of matrix phase is preferred for higher toughness at low temperature, the comparison of the Charpy impact toughness between fresh martensite which is a product of the re-transformation of the austenitic phase and tempered martensite structure was carried out. Direct comparison of the as-quenched condition (Q) to the as-quenched and tempered

condition (QT) in Table V is not reasonable for this purpose, since any thermal process after austenitizing changes not only the matrix from fresh martensite to tempered martensite but also the grain size through polygonization. In order to exclude the effect of grain size on the mechanical properties, tempered martensite matrix which was obtained by the QLT treatment for the Fe-6Ni base alloy and the QT treatment for alloy M and commercial Fe-9Ni alloy was rapidly heated up to 850°C (slightly above A_f transformation temperature) in an induction furnace and then quenched immediately into ice brine (up-quenching process) as designated in Fig. 1. The up-quenching process was conducted within a very short time (around 12 seconds).

Figure 19 shows the transmission electron micrograph of as-quenched and tempered (QT) commercial Fe-9Ni alloy. As shown in the micrograph, the QT treated specimen consists of retained austenite and polygonized tempered martensite. X-ray diffraction for this alloy revealed that about 12.7 pct of retained austenite was present. Figure 20 shows a corresponding transmission electron micrograph of an up-quenched Fe-9Ni alloy. The up-quenched alloy has a highly dislocated lath martensite structure. The trace of the polygonized subgrains found in the QT treated tempered martensite structure is still visible in the up-quenched lath martensite structure. But dislocation networks on polygonized subgrain boundaries were a little blurred. However, retained austenite phase was not detected at all in up-quenched specimens in either transmission electron microscopic and x-ray diffractometric studies. In order to obtain the more stable retained austenite phase prior to up-quenching treatment, 100 hours tempering was conducted, but the retained austenite phase was still transformed to martensite.

The Charpy impact properties of the QT and up-quenching treated Fe-9Ni alloy are presented in Fig. 21(b). As seen in this figure, use of the up-

quenching process decreased the upper shelf energy of Charpy impact and increased the ductile-brittle transition temperature. Figures 22 and 23 show the fractographs of QT and corresponding up-quenched commercial Fe-9Ni alloy, respectively. Both fractographs show the ductile dimple fracture mode at room temperature, but the brittle quasi-cleavage fracture mode at liquid nitrogen temperature.

An almost similar behavior was observed in the Fe-6Ni base alloy by the up-quenching process, as shown in Fig. 21(a). The upper shelf energy of Charpy impact in the up-quenched base alloy was decreased and the transition temperature was increased. The latter is evident from the fractographs. As shown in Figs. 24(a) and (c), the ductile dimple fracture mode for room temperature appeared in both QLT treated and corresponding up-quenched base alloy. However, as shown in Figs. 24(b) and (d), the QLT treated base alloy was fractured by a complete ductile dimple mode while the up-quenched alloy was fractured by a mixture of dimple and quasi-cleavage modes. This observation revealed that the up-quenching process for the base alloy surely increased the transition temperature. This result is quite consistent with that of commercial Fe-9Ni alloy as described previously.

A similar comparison was achieved in alloy M where no retained austenite phase was presented in the QT treated condition. For the alloy M, the real comparison of mechanical properties between tempered martensite and lath martensite matrix without the presence of retained austenite at nearly the same grain size was possible. Figure 21(c) shows the Charpy impact energy with respect to test temperature for alloy M. As shown in Fig. 21(c), the transition temperature was not affected at all. This observation differs somewhat from that found in the base alloy and the commercial Fe-9Ni alloy. However, the upper shelf energy of Charpy impact was slightly decreased.

This result is rather consistent with that in the base alloy and that in Fe-9Ni alloy even though the degree of decrease is smaller than the base alloy and Fe-9Ni alloy. When the fact that both the base alloy and Fe-9Ni alloy have 0.06 pct carbon, while alloy M has 0.001 pct carbon, is considered, this difference of its discrepancy seems due to the carbon content in the alloys.

Tables VI and VII show the mechanical properties at room temperature and liquid nitrogen temperature of Fe-6Ni base alloy and alloy M which meet the difference between tempered martensite and lath martensite. Table VI shows that the yield and ultimate tensile strengths of up-quenched Fe-6Ni base alloy after the QLT treatment are nearly twice as high as those of QLT heat treatment, while those of alloy M are not changed so much, as shown in Table VII. The increase in the properties seems due to the introduction of higher dislocation density in up-quenched alloys by the up-quenching process. The discrepancy of its severity between the base alloy and alloy M seems due to the difference of carbon content and the existence of retained austenite phase as discussed in the latter part.

Furthermore, as can be seen in Tables V and VI, the identical three-step QLT heat treatment, comparable impact toughness to that of the base alloy at liquid nitrogen temperature was not obtained in the alloy M. Yield and ultimate tensile strengths of the base alloy were higher than those of alloy M. This discrepancy also seems due to the same reason as described previously.

These observations reveal that the low temperature properties of the matrix, which occupies most of the final microstructure of the base alloy, is not responsible for those of the base alloy.

IV. DISCUSSION

A. Stability of Retained Austenite.

Retention of stable austenite phase in ferritic steel has been consi-
dered very important for low temperature toughness[10,13,26-32] since only
stable austenite has shown beneficial effect on the toughness.[18-20] The
stability of retained austenite in ferritic steel is believed to be a
function of the initial chemical composition[28,29,33] and presumed to be
aided by stress generated by phase transformation resulting in volume
changes.[24,34] It has been noted,[35] that for a given deformation tempera-
ture, the austenite stability is a function of the alloy composition and
thermomechanical history. Austenite of a given composition can be further
stabilized by mechanical[33] and/or thermal[34] treatments. Large amounts of
deformation of the austenite increase its dislocation density and thus in-
hibit a martensitic transformation. On the other hand, thermal treatments
allow interstitial atoms to lock mobile dislocations and thus increase the
austenite stability.

The composition of alloy A in this research is based on the previous
work of scanning transmission electron microscopy analysis of the composi-
tion of the retained austenite in QLT treated Fe-6Ni alloy.[20] There is no
doubt that high Ni, Mn, Mo, and Cr contents in the retained austenite phase
lower the martensitic transformation temperature (M_s temperature). However,
the decrease in M_s temperature by enrichment of substitutional alloying ele-
ments is rather small when compared with that by carbon. Steven and Haynes[36]
suggested that M_s temperatures can be calculated approximately by the fol-
lowing equation: $M_s(°C) = 561 - 474C(\%) - 33Mn(\%) - 17Ni(\%) - 21Mo(\%)$. In
fact, the M_s temperature of alloy A is expected to decrease by 334°C due to
the total amounts of Ni, Mn, Mo, and Cr in alloy A, as designated in Table I,

while only 0.42 pct carbon lowers the M_s temperature by 199°C.

It is still unclear, however, that retained austenite in a OLT treated base alloy can be stable at liquid nitrogen temperature by chemical composition alone, since the precise determination of carbon content in the austenite was not conducted, and is, in fact, impossible at this moment. But a theoretically calculated mean distance of diffusion of carbon during the intercritical tempering (600°C/1 hr.) is estimated to be about 350 μm while a mean distance between retained austenite islands is only about 1 μm.[20] Considering that many dislocations and/or free surfaces exist, the mean distance of diffusion of carbon in ferritic steel can be greater than that of this theoretical value. Therefore, a mean distance of diffusion of carbon during tempering is sufficiently greater than the distance between retained austenite islands. Hence, it is likely that the retained austenite in the Fe-6Ni base alloy contains carbon at its maximum solubility, so that it is reasonable that the retained austenite contains such a carbon of 0.42 pct.

It was previously proposed[37,38] that thermal stabilization of austenite occurs because of an anchoring effect of the segregated carbon atoms inhibiting the activation of the martensite embryos into propagating martensite plates. Fahr[34] also showed that the stability of retained austenite was controlled by varying the amount of carbon so that increasing carbon content increased the austenite stability. As described previously in the present research, the austenitic alloy A which had 0.42 pct carbon was transformed to martensite only about 25 pct and 56 pct by quenching to liquid nitrogen temperature and liquid helium temperature, respectively. The chemical segregation in retained austenite seems adequate to stabilize the austenite phase at liquid nitrogen temperature without considerable influence by other

factors such as stress, although precise examination of interstitial content in retained austenite should be considered.

B. Role of Retained Austenite.

It is well established[13,13,26] that the retained austenite phase in ferritic steels scavenges interstitial impurities out of the matrix resulting in an improvement of mechanical properties. However, such an effect of retained austenite is noted only if the alloy contains interstitials such as carbon to be scavenged. It was reported[15,16] that interstitial-free cryogenic steels were still tough even though retained austenite was absent. In these cases the excellent toughness of cryogenic alloys is due to the interstitial-free matrix but not due to the toughness of retained austenite phase itself. In this research, as shown in Table IV, the Charpy impact energy of alloy A is only 9.3 ft-lb (12.6 Joule) at liquid nitrogen temperature while that of Fe-6Ni base alloy is 131.3 ft-lb (178.6 Joule) at an identical test temperature. This result shows that toughness of the retained austenite phase has a minor role in an overall cryogenic toughness of the base alloy.

However, an alternative explanation of the beneficial effect of the stable retained austenite other than the scavenging effect is still very plausible. As described previously, the grain refinement of alloy M suppressed the ductile-brittle transition temperature, while the upper shelf energy of Charpy V-notch impact was not affected at all: see Fig. 6. However, changing the matrix from tempered martensite to highly dislocated lath martensite in the alloy M turned out to slightly decrease the upper shelf energy, as shown in Fig. 21(c). On the other hand, changing the matrix from a mixture of tempered martensite and retained austenite to lath

martensite in Fe-6Ni base alloy and commercial Fe-9Ni alloy appeared to not only decrease the upper shelf energy but also to increase the transition temperature as described in Figs. 22(a) and (b). The discrepancy in the transition temperature in the latter case is obviously coming from the existence of retained austenite phase in the ferritic matrix. Therefore, the existence of retained austenite in the Fe-6Ni base alloy and Fe-9Ni alloy induces the grain refinement of those alloys. Thus, the retained austenite can act as a grain refiner. This result is quite consistent with the proposal of Morris, et al.[8] They showed that the strain-induced transformation of the retained austenite resulted in a martensite of different orientation from that of the ferrite matrix, hence, preserving a grain refinement conducive to low temperature toughness. As described previously, the toughness of retained austenite phase itself seems unimportant to the overall toughness of ferritic steel. However, the austenite is thermally stable by composition itself but mechanically unstable. If it is transformed by plastic deformation generated by crack propagation as in the Morris, et al. model, it transforms to a martensite phase of different orientation from that of the neighboring ferrite matrix resulting in a rather effective grain refinement.

C. Effect of Carbon on Grain Size and Charpy Impact Properties.

The grain size referred to in Fig. 5 indicates the average size of the smallest unit area appearing in an etched specimen. The grain size for this microstructure was determined by the linear-intercept method. Transmission electron microscopy studies show that the unit area in optical micrographs indicates either a cell of mixed boundaries composed of fresh martensite, which is a product of the re-transformation of austenite and tempered

martensite, or a polygonized subcell which forms a redistribution of dislocations in the tempered martenstie matrix. It has not been well established if the polygonized substructure would be regarded as a unit grain which influences mechanical properties as prior austenite grains in a typical martensitic steel do. As shown in Fig. 6, however, the polygonized substructure appears to influence the ductile-brittle transition temperature more or less, although it would rather depend on the degree of relative misorientation of adjacent subgrains.

No matter how much grain size contributes to mechanical property, the size of the subcell in alloy M appears much coarser than that in the Fe-6Ni base alloy, even though identical heat treatments were conducted.[20] Furthermore, 50 pct cold-working of alloy M followed by QLT heat treatment was not sufficient to produce a grain size identical to that achieved by QLT treatment alone in the base alloy. This observation seems to be due to the effect of carbon on grain refinement. Even if it is not well understood, as described previously, the high diffusivity of carbon seems to facilitate the nucleation and growth of the austenite phase so that it leads to efficient grain refining during heat treatment.

The carbon content in the Fe-6Ni base alloy and Fe-9Ni alloy appeared to affect not only grain refining but also the Charpy impact energy and stability of retained austenite. Similar observations[20,34,38] of a decrease in Charpy impact energy due to carbon are reported in many alloys. However, Niikura and Morris[39] found that an increase of carbon content in ferritic 5Mn steel deteriorated the impact toughness. When carbon is coupled with dislocations generated by martensitic transformation, it might be a source of deteriorating Charpy impact energy. But, if the austenite phase is formed during the following tempering process, so that the deleterious

carbon is scavenged from the matrix, the overall Charpy impact energy increases again very significantly. The influence of carbon, although not great, seems beneficial for controlling the transition temperature, since it can reduce the grain size and promote formation of stable austenite, resulting in grain refinement.

D. Metallurgical Source of Excellent Cryogenic Properties of Ferritic Fe-6Ni Alloy.

As a result of the present work, it was found that retained austenite itself in the ferritic Fe-6Ni alloy was not a source of the high impact toughness of the base alloy at either room temperature or liquid nitrogen temperature. The low temperature properties of the matrix which occupies most of the final microstructure of ferritic Fe-6Ni alloy was also not responsible for the properties of the base alloy. However, this present work also showed that refining the grain size suppressed the transition temperature very effectively. Therefore, if the grain size of alloy M is refined identically to that of the Fe-6Ni base alloy, since alloy M is nearly an interstitial-free alloy and very tough in its ductile region as shown in Fig. 6, it seems possible that alloy M may be tough at cryogenic temperature. However, even though the alloy was treated by the identical thermal cycling to that of the base alloy, its grain size appeared to be larger than that of the base alloy. Furthermore, the cold-worked alloy M before the QLT heat treatment did not achieve grain sizes identical to those of the base alloy with the identical heat treatment and no cold working. As described previously, the difference in sensitivity to grain refinement between alloy M and the base alloy seems to be the effect of carbon content on grain refinement.

Through the introduction of an admixture of thermally stable austenite phase in the ferritic steel, excellent cryogenic properties were achieved. That is, it is more likely that excellent cryogenic properties are obtainable by the combined effects of each microstructural component of the alloy.

V. CONCLUSION

1. The grain size of the alloy does not affect the upper shelf energy of Charpy V-notch impact. However, the ductile-brittle transition temperature is suppressed by the grain refinement. Grain refinement seems to be achieved by the formation of stable retained austenite phase, as well as polygonized subgrains in the matrix.

2. The retained austenite phase in three-step QLT treated Fe-6Ni alloy seems to be thermally stable by composition itself. Thermally stable austenite, however, easily transformed under applied strain.

3. The retained austenite phase is not a tough phase. However, the introduction of retained austenite phase in ferritic steel increases cryogenic toughness of the alloy by either scavenging deleterious impurities or grain refinement.

4. The martensitic matrix of the ferritic steel has no effect on the transition temperature. However, a matrix of tempered martensite is preferable to dislocated lath martensite for enhancement of the upper shelf energy of Charpy impact.

5. An excellent cryogenic toughness can be obtained by the combined effects of each microstructural component of the alloy.

REFERENCES

1. T. Ooka, H. Mimura, S. Yano, K. Sugibo, and T. Toizumi: J. Jpn Inst. Metals, 1966, 30, 442.

2. H. Sakurai, S. Yano, T. Inoue, H. Mimura, and K. Aoki: J. Jpn Inst. Metals, 1969, 33, 856.

3. G. L. Swales and A. G. Haynes: Metal Progress, June, 1975, 43.

4. S. Nagashima, T. Ooka, S. Sekino, H. Mimura, T. Fujishima, S. Yano, and H. Sakurai: Trans. Iron Steel Inst. Jpn., 1971, 11, 402.

5. S. Nagashima, T. Ooka, S. Sekino: Tesu-to-Hagane, 1972, 58, 128.

6. S. Yano, H. Sakurai, H. Mimura, N. Wakita, T. Ozawa, and K. Aori: Trans. Iron Steel Inst. Jpn., 1973, 13, 133.

7. C. W. Marshall, R. F. Heheman, and A. R. Troiano: Trans. ASM, 1962, 55, 135.

8. J. W. Morris, Jr., C. K. Syn, J. I. Kim, and B. Fultz: Proc. Int. Conf. on Martensitic Transformations (ICOMAT), Cambridge, MA, June, 1979, 572.

9. S. K. Hwang, S. Jin, and J. W. Morris, Jr.: Met. Trans., 1975, 6A, 2015.

10. C. K. Syn, S. Jin, and J. W. Morris, Jr.: Met. Trans., 1976, 7A, 1827.

11. T. Ooka and K. Sugiano: J. Jpn. Inst. Metals, 1966, 30, 435.

12. S. Jin, S. K. Hwang and J. W. Morris, Jr.: Met. Trans., 1975, 6A, 1721.

13. J. I. Kim and J. W. Morris, Jr.: Met. Trans., 1980, 11A, 1401.

14. K. J. Kim and L. H. Schwartz: Mat. Sci. Eng., 1978, 33, 5.

15. S. Jin, J. W. Morris, Jr., and V. F. Zackay: Met. Trans., 1975, 6A, 141.

16. S. Jin, S. K. Hwang, and J. W. Morris, Jr.: ibid, 1569.

17. D. Hardwick: Iron Steel, 1961, 34, 414.

18. C. A. Pampillo and H. W. Paxton: Met. Trans., 1972, 3, 2895.

19. C. K. Syn, B. Fultz, and J. W. Morris, Jr.: Met. Trans., 1978, 9A, 1635.

20. J. I. Kim: Ph.D. Thesis, University of California, Berkeley, #LBL-9956, 1979.

21. R. L. Miller: Trans. ASM, 1964, 57, 892.

22. R. L. Miller: Met. Trans., 1972, 3, 905.

23. G. Saul, J. A. Roberson, and A. M. Adair: Met. Trans., 1969, 1, 383.

24. G. R. Chanani, V. F. Zackay, and E. R. Parker: Met. Trans., 1971, 2, 133.

25. B. Karlsson: Mat. Sci. Eng., 1973, 11, 185.

26. C. W. Marshall, R. H. Heheman, and A. R. Troiano: Trans. ASM, 1962, 55, 135.

27. D. Webster: Met. Trans., 1971, 2, 2097.

28. D. Bhandarkar, V. F. Zackay, and E. A. Parker: Met. Trans., 1972, 3, 2619.

29. C. A. Pampillo and H. W. Paxton: Met. Trans., 1972, 3, 2895.

30. H. Haga: Trans. Iron Steel Inst. Jpan., 1973, 13, 141.

31. S. Antolovich, A. Saxena, and G. R. Chanani: Met. Trans., 1974, 5, 623.

32. G. Y. Lai, W. E. Wood, R. A. Clark, V. F. Zackay, and E. R. Parker: Met. Trans., 1974, 5, 1663.

33. J. R. C. Guimarages and J. C. Shyne: Met. Trans., 1971, 2, 2063.

34. D. Fahr: Met. Trans., 1971, 2, 1883.

35. K. R. Kinsman and J. C. Shyne: Acta Met., 1966, 14, 1063.

36. W. Steven and A. G. Haynes: J. Iron. Steel Inst., 1956, 183, 349.

37. K. R. Kinsman and J. C. Shyne: Acta Met., 1967, 15, 1527.

38. D. Webster: Met. Trans., 1970, 2, 1857.

39. M. Niikura and J. W. Morris, Jr.: Met. Trans., 1980, 11A, 1531.

TABLE I. Chemical Composition of Alloys. (Unit: Wt pct)

	Fe	C	Mn	Si	P	S	Ni	Cr	Mo
Fe-6Ni	Bal.	0.063	1.21	0.20	0.08	0.01	5.86	0.69	0.20
Retained Austenite*	Bal.	0.50**	3.90	0.30	-	-	9.00	2.10	2.0***
Tempered Martensite*	Bal.	0.01**	0.60	0.19	-	-	5.00	0.08	0.34***
Alloy A	Bal.	0.42	3.29	0.19	0.002	0.005	9.61	1.16	2.01
Alloy M	Bal.	0.021	0.57	0.18	0.001	0.006	4.98	0.09	0.31

* Scanning transmission electron microcopy analysis data[20].

** Theoretically calculated data.

*** Chemical extraction data[20].

TABLE II. Transformation Temperatures of Alloy M.

	A_s	A_f	M_s	M_f
Temperature (°C)	735	765	590	540

TABLE III. Mechanical Properties at Room Temperature of

Thermomechanically Treated Alloy M.

Cold Working	0%	25%	50%
Y. S. (Ksi) (MPa)	67.9 (468.0)	69.4 (479.0)	72.1 (497.0)
U. T. S. (Ksi) (MPa)	82.3 (567.0)	81.9 (565.0)	83.1 (573.0)
Total Elong. (%)	35.2	35.3	34.6
R. A. (%)	85.7	86.9	83.8
C_v. (ft-lb) (Joule)	216.4 (293.2)	217.2 (294.3)	216.9 (293.9)

(Note) Thermomechanical Treatment: X(%) Cold working +
800°C/1 hr. + 670°C/1 hr. + 600°C/1 hr. (Water
quenched after each heat treatment.)

TABLE IV. Mechanical Property of Alloy A and Fe-6Ni Alloy.

	Alloy A		Fe-6Ni
	R.T.	-196°C	-196°C
Y. S. (Ksi)	61.1	83.9	139.4
(MPa)	(421.0)	(578.0)	(961.0)
U. T. S. (Ksi)	*	*	170.1
(MPa)			(1173.0)
Fract. S. (Ksi)	179.2	313.6	**
(MPa)	(1236.0)	(2162.0)	
Total Elong. (%)	36.4	28.4	31.5
R. A. (%)	31.8	22.6	67.4
C_v. (ft-lb)	39.2	9.3	131.8
(Joule)	(53.1)	(12.6)	(178.6)

(Note) * not measurable.
      ** not tested.

TABLE V. Mechanical Properties of Alloy M.

Test Temperature	800°C/1 hr.		800°C/1 hr. +600°C/1 hr.		800°C/1 hr. +670°C/1 hr. +600°C/1 hr.		800°C/1 hr. +710°C/1 hr. +600°C/1hr.	
	R.T.	-196°C	R.T.	-196°C	R.T.	-196°C	R.T.	-196°C
Y. S. (Ksi)	75.8	122.2	72.8	126.3	67.9	115.7	67.4	121.6
(MPa)	(523.0)	(843.0)	(502.0)	(871.0)	(468.0)	(798.0)	(465.0)	(838.0)
U. T. S. (Ksi)	88.5	150.0	84.8	137.7	82.3	131.1	83.0	132.4
(MPa)	(610.0)	(1034.0)	(585.0)	(949.0)	(567.0)	(904.0)	(572.0)	(910.0)
Total Elong. (%)	30.4	30.8	31.4	33.4	35.2	39.7	35.6	42.2
R. A. (%)	82.7	73.8	84.9	74.3	85.7	75.5	85.1	75.3
C_v. (ft-lb)	196.5	8.1	217.2	10.2	216.4	14.0	217.2	7.2
(Joule)	(266.3)	(11.0)	(294.3)	(13.8)	(293.2)	(19.0)	(294.3)	(9.6)

(Note) Water-quenched after each heat treatment.

TABLE VI. Mechanical Properties of Fe-6Ni Base Alloy

Test Temperature	QLT		QLT + UQ	
	R.T.	-196°C	R.T.	-196°C
Y. S. (Ksi)	93.7	139.4	172.1	224.6
(MPa)	(646.0)	(961.0)	(1187.0)	(1549.0)
U. T. S. (Ksi)	114.5	170.1	190.2	237.5
(MPa)	(789.0)	(1173.0)	(1311.0)	(1638.0)
Total Elong. (%)	28.9	31.5	17.1	19.6
R. A. (%)	80.1	67.4	66.6	64.8
C_v. (ft-1b)	179.4	131.8	70.0	29.0
(Joule)	(243.1)	(178.6)	(94.9)	(39.3)

(Note) QLT: 800°C/1 hr. + 670°C/1 hr. + 600°C/1 hr
              (Water-quenched after each heat treatment.)

        UQ: Up-quenching process.

TABLE VII. Mechanical Properties of Alloy M.

	QT		QT + UQ	
	R.T.	-196°C	R.T.	-196°C
Y. S. (Ksi)	72.8	126.3	85.6	128.4
(MPa)	(502.0)	(871.0)	(590.0)	(885.0)
U. T. S. (Ksi)	84.8	137.7	95.3	148.3
(MPa)	(585.0)	(849.0)	(657.0)	(1023.0)
Total Elong. (%)	31.4	33.4	24.9	24.3
R. A. (%)	84.9	74.3	84.3	73.3
C_v. (ft-1b)	217.2	10.2	209.1	8.2
(Joule)	(294.3)	(13.8)	(283.3)	(11.1)

(Note) QT: 800°C/1 hr. + 600°C/1 hr. (Water-quenched after each heat treatment.)

UQ: Up-quenching process.

FIGURE CAPTIONS

1. Schematic diagram of up-quenching thermal process adopted in the present research.

2. Standard dilatometry test specimen for measuring phase transformation temperatures.

3. Cylindrical compact tensile test specimen.

4. Standard Charpy V-notch impact test specimen.

5. Optical micrographs of cold-worked alloy M by (a) 0 pct, (b) 25 pct, and (c) 50 pct., respectively followed by QLT (800°C/1 hr. + 670°C/1 hr. + 600°C/1 hr.) heat treatment.

6. Depression of ductile-brittle transition temperature by thermomechanical treatment which is cold-worked followed by QLT (800°C/1 hr. + 670°C/1 hr. + 600°C/1 hr.) heat treatment.

7. Optical micrographs of alloy A at (a) room temperature and (b) liquid nitrogen temperature (-196°C) for the same area.

8. Optical micrographs of alloy A at (a) room temperature and (b) liquid helium temperature (-269°C).

9. TEM micrographs of annealed (900°C/2 hrs.) and austenitized (800°C/1 hr.) alloy A.

10. TEM micrograph of solution-annealed (900°C/2 hrs.) and austenitized (800°C/ 1 hr.) alloy A showing the (1$\bar{1}$1) twin plane.

11. TEM micrograph of alloy A showing carbide precipitates at austenite grain boundaries. Letters M and P denote the matrix and precipitate phase, respectively.

12. Optical micrograph of cross-section of Charpy impact test alloy A broken at room temperature.

24. SEM fractographs of QLT treated Fe-6Ni base alloy broken at (a) room temperature and (b) liquid nitrogen temperature (-196°C) and QLT treated and then up-quenched the alloy broken at (c) room temperature and (d) liquid nitrogen temperature.
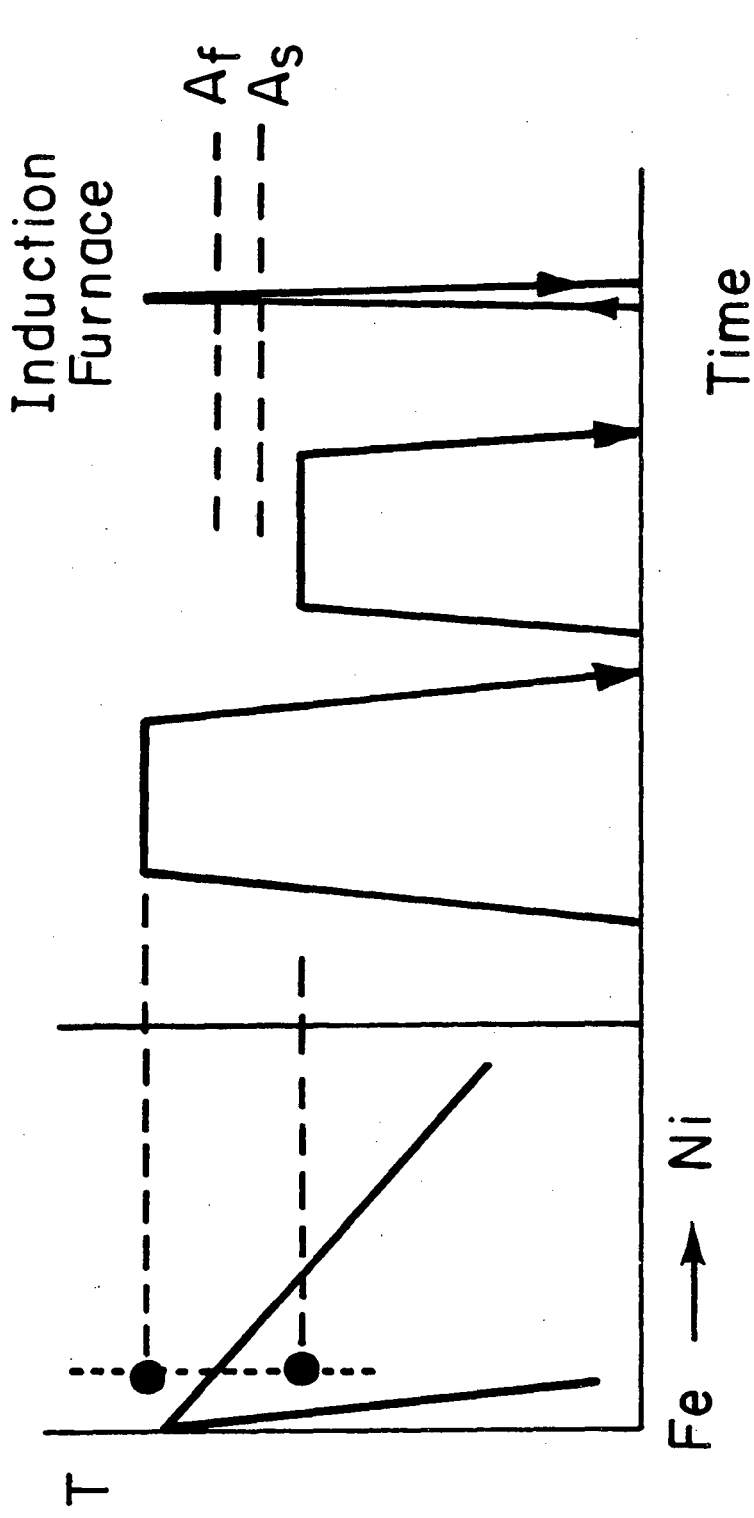
Fig. 1.

XBL 807-10701A

XBL 79IO-7192

0.394"

0.188" 0.125"

Fig. 2.

28 thds/inch

0.250"

0.500"

0.125"

0.563"

1.750"

0.500"

XBL 774-5354

Fig. 3.

45°

0.079" ± .001 (2mm)

Notch radius 0.01"(0.25mm)

0.315" (8mm)

0.394"
±.001

2.165"
(55 mm)

0.394"±.001
(10 mm)
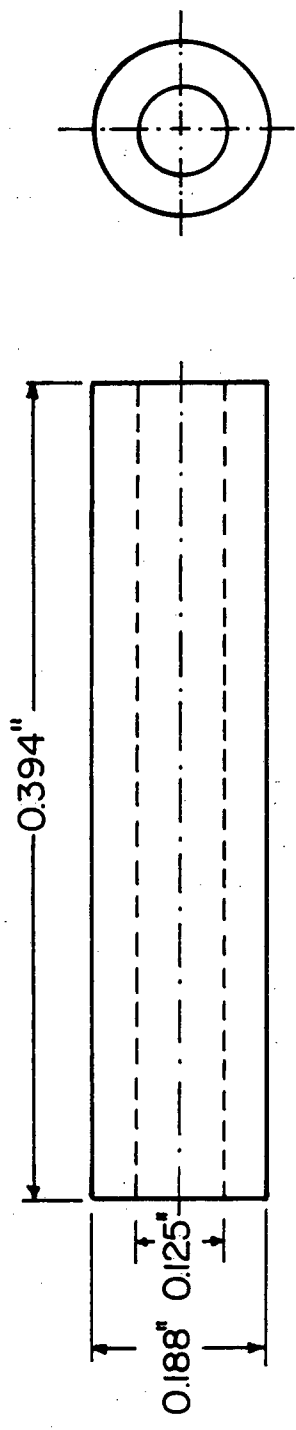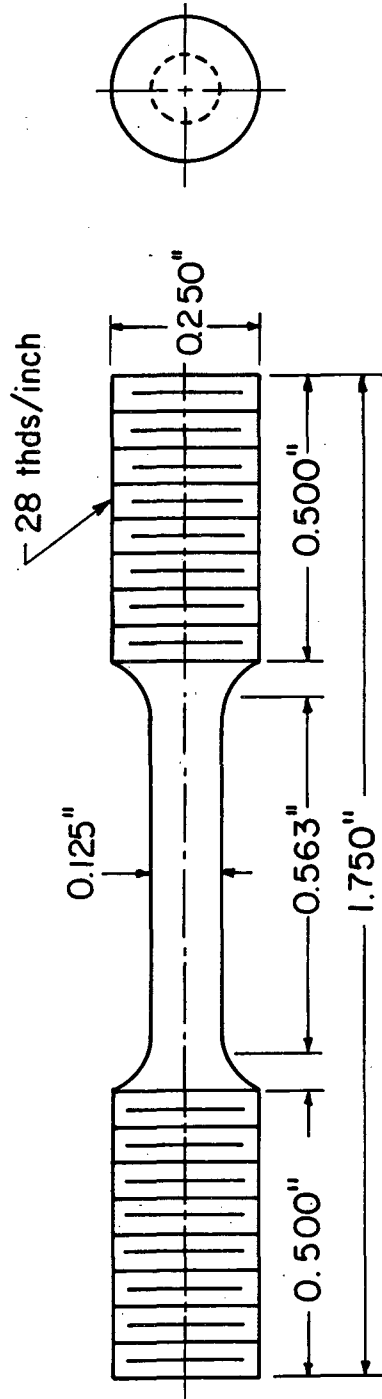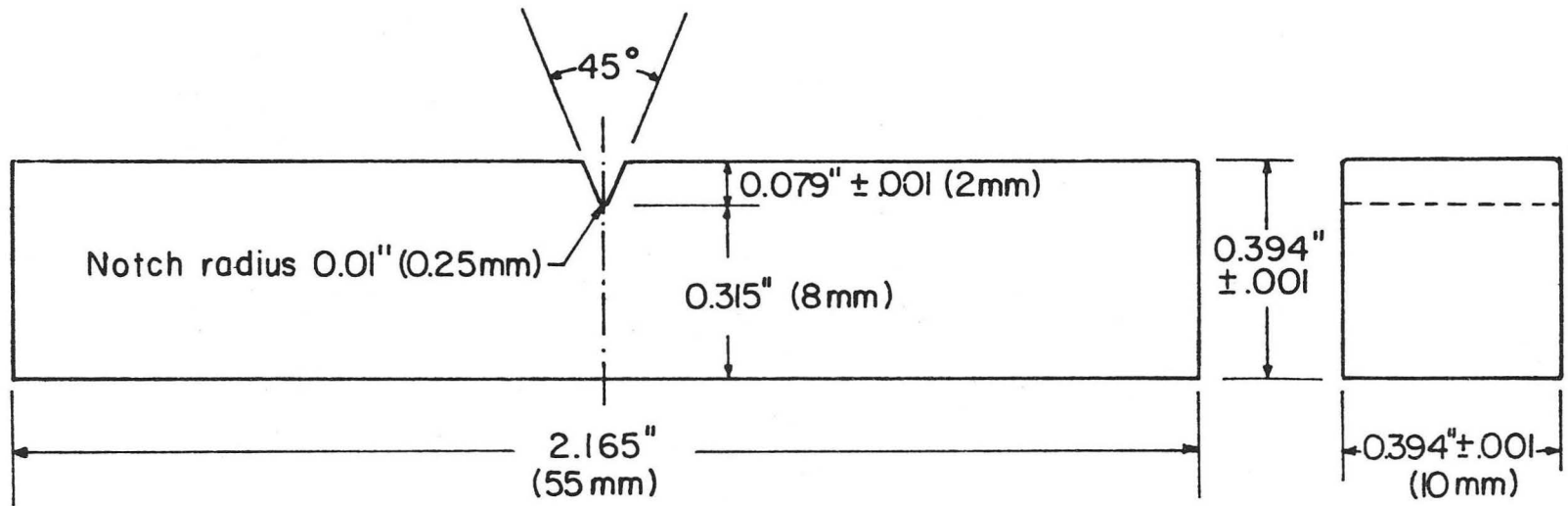
Grind finish

Fig. 4.
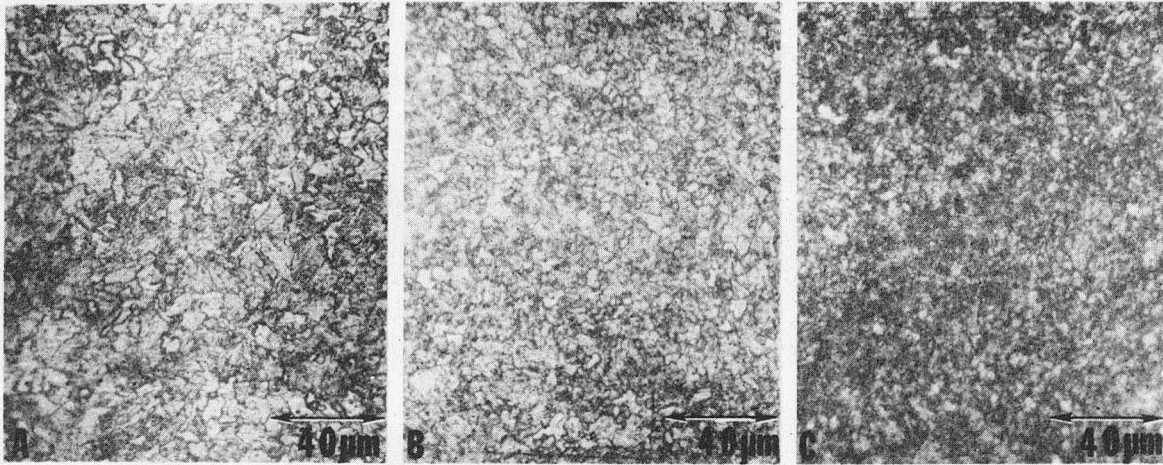
0 %   25 %   50 %

X % C.W. + QLT

XBB 809-11265

Fig. 5.
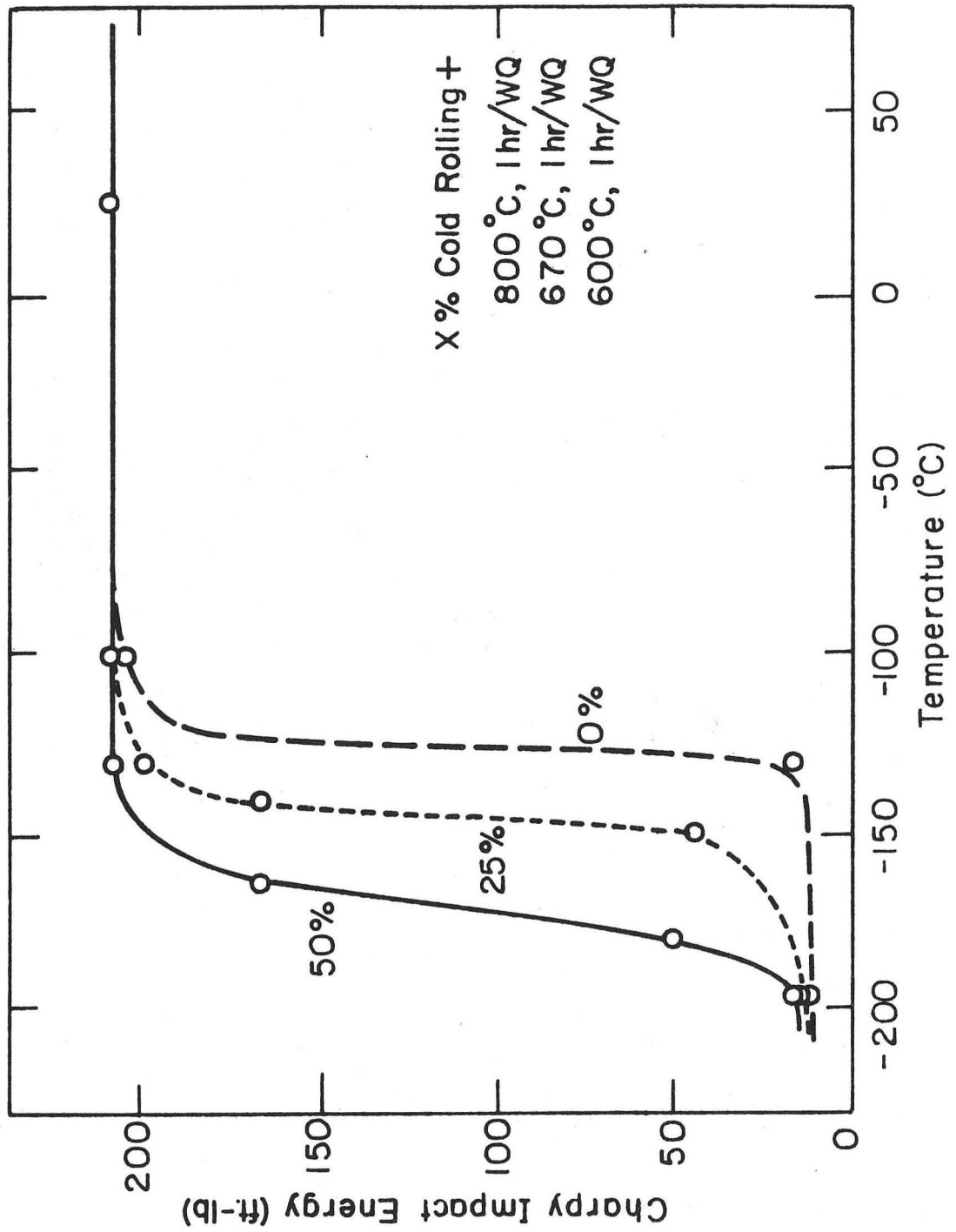
Fig. 6.

XBL 809-5937
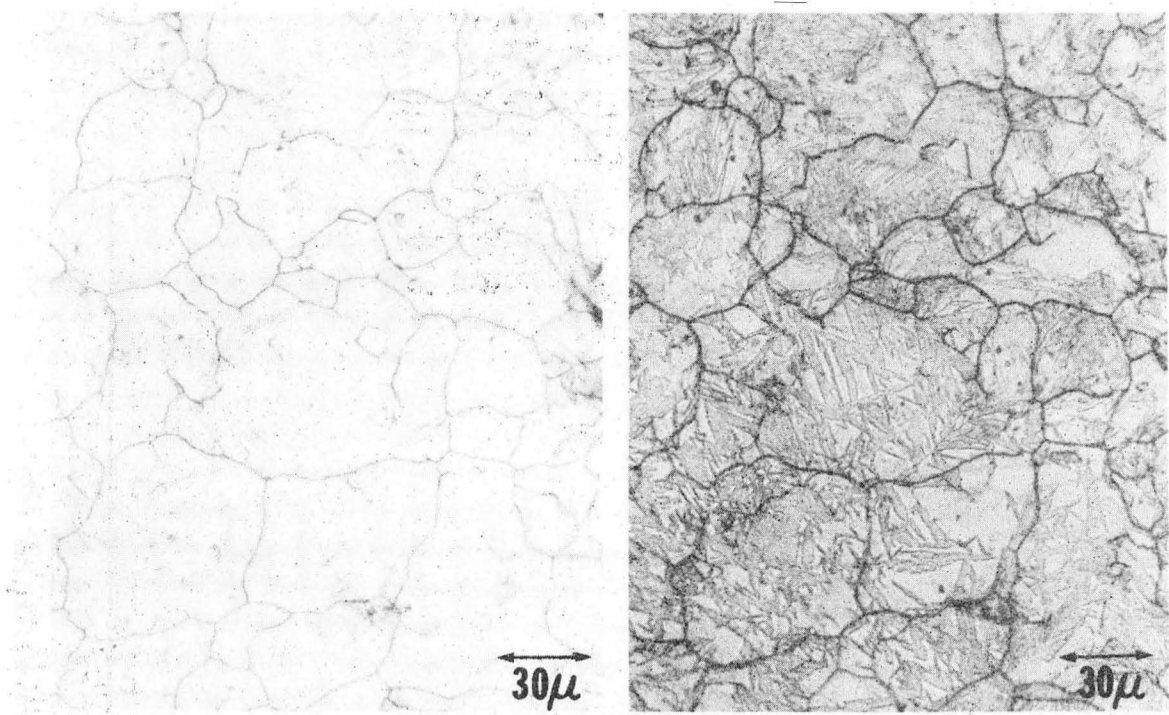
R.T.　　　　　　　　L.N.T.

Fig. 7.

A

A+M

XBB 807-8901

Fig. 8.

(002)

(1Ī1)

(Ī11)

(1ĪĪ)

(Ī1Ī)

(00Ī)

● (110) Austenite

XBB 806-7277

Fig. 9.

Fig. 10.

XBB 806-7278

Fig. 11.

200μm

Notch
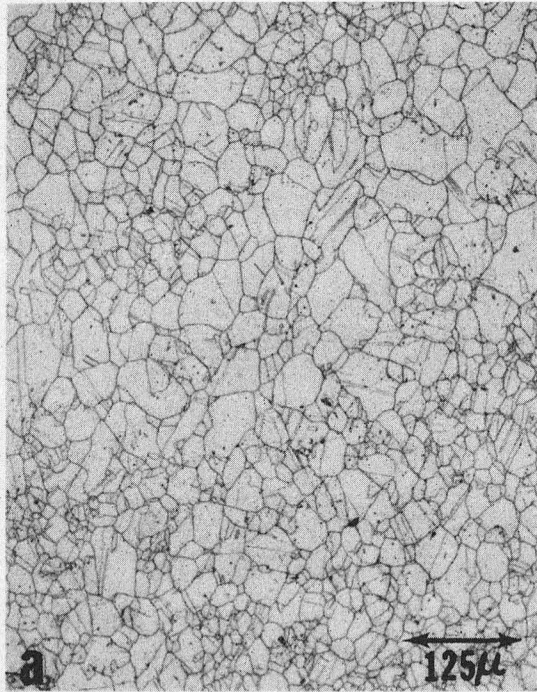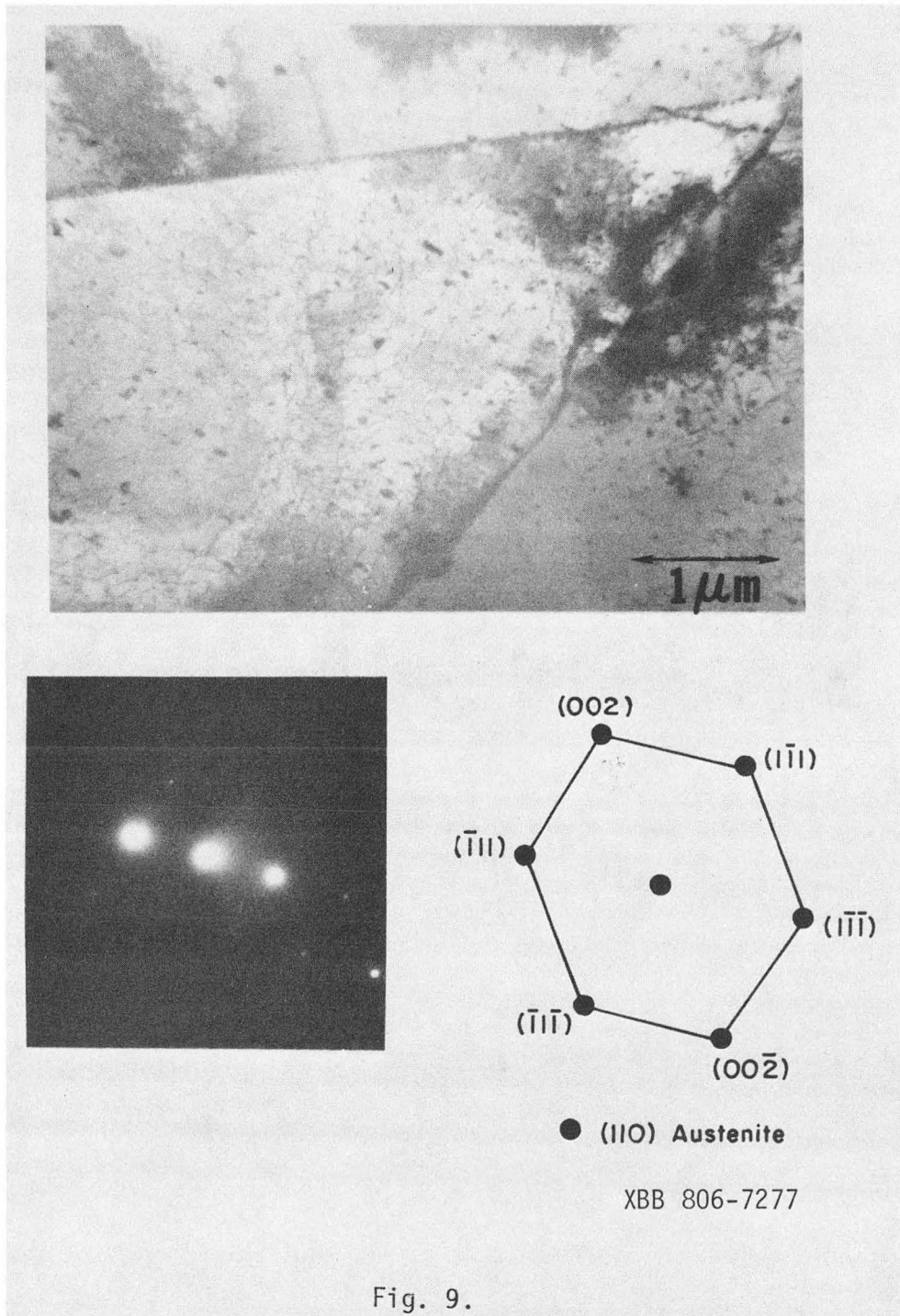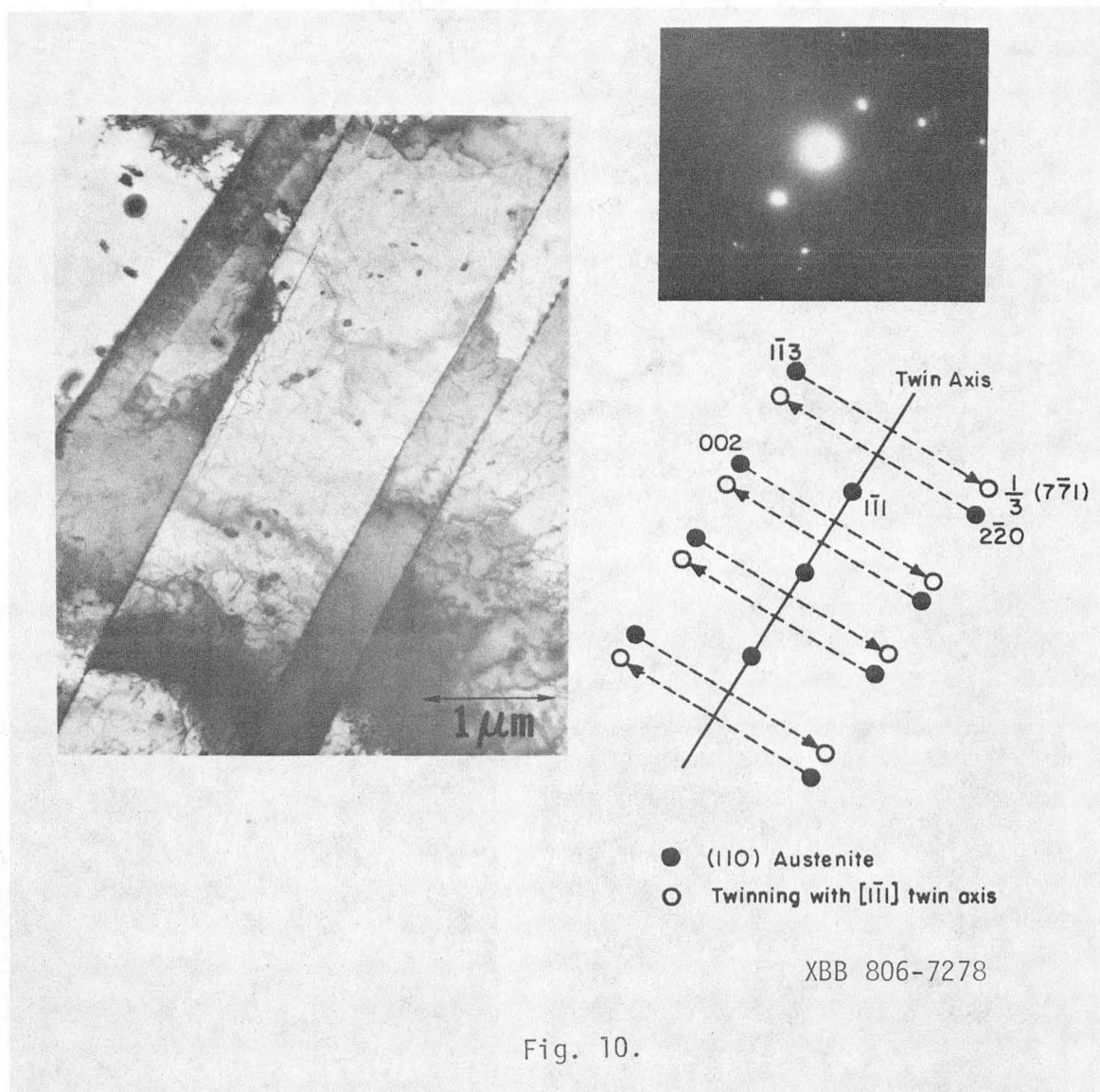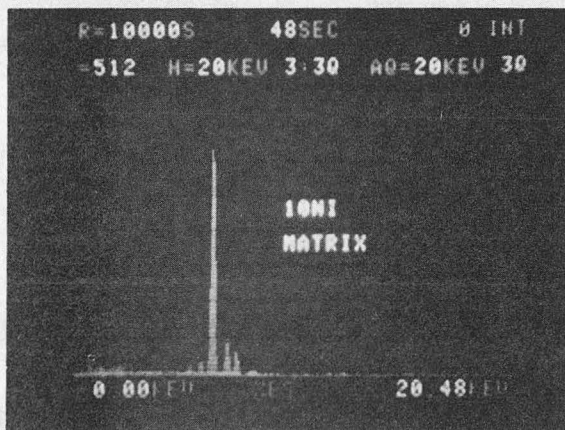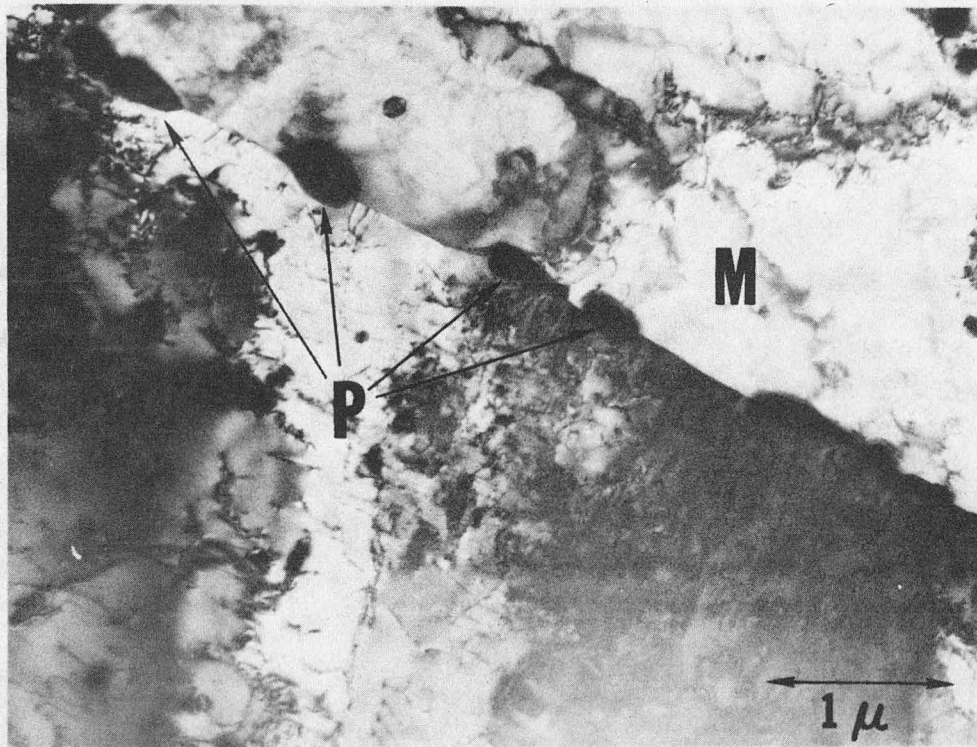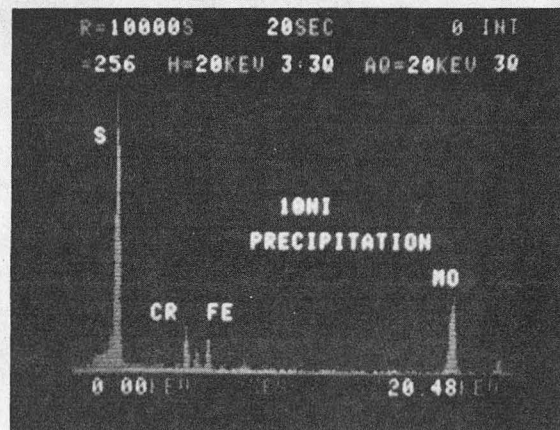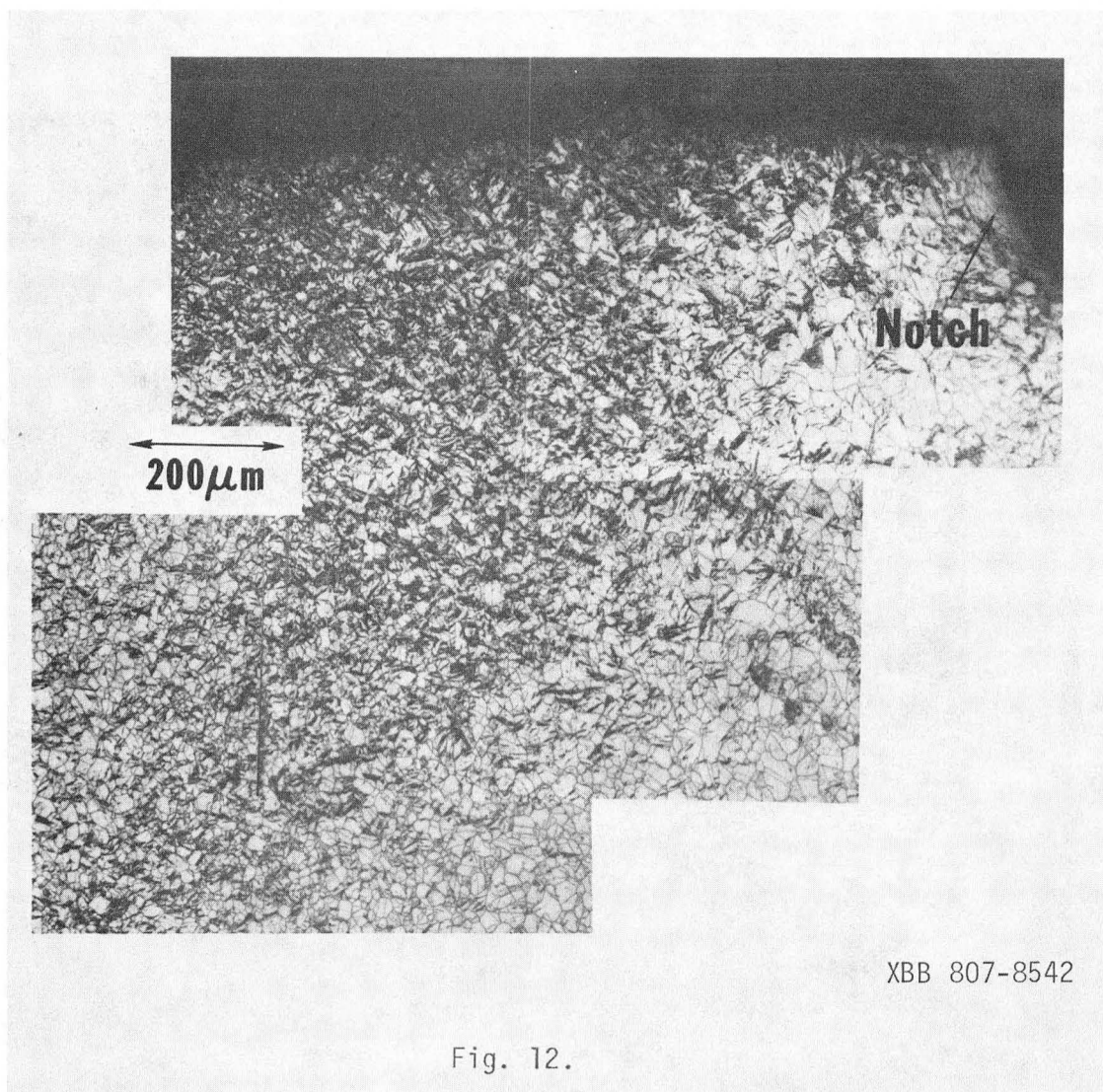
XBB 807-8542

Fig. 12.
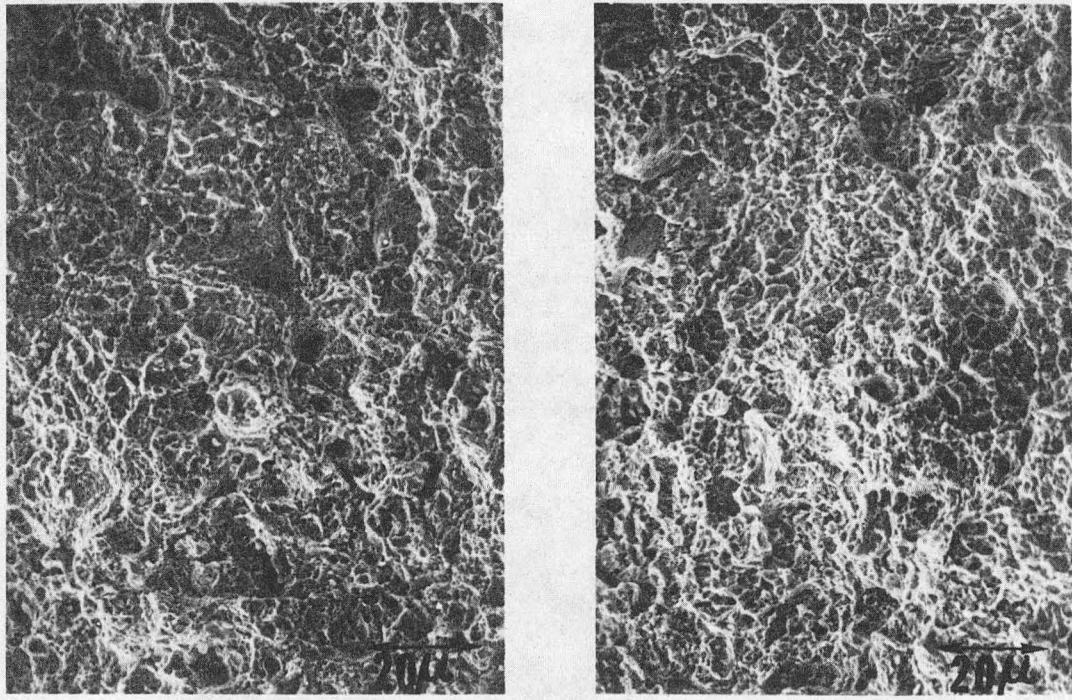
A   A+M

(RT)

XBB 807-8540

Fig. 13.
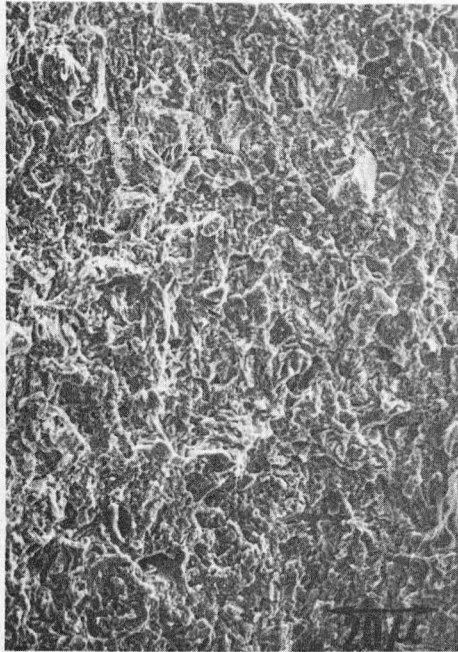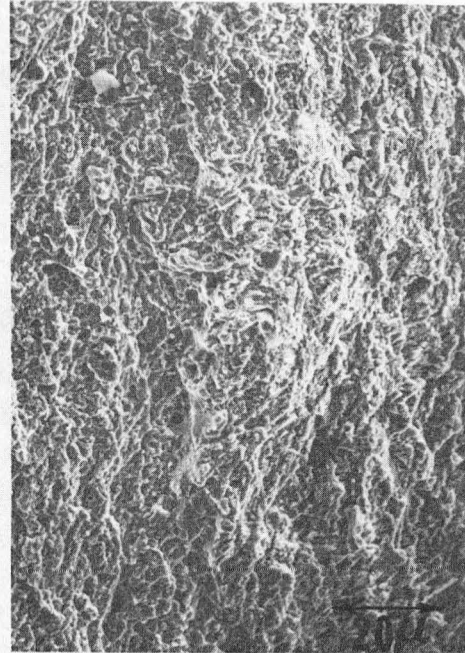
A + .25 M   A + .56 M

(LNT)

XBB 807-8541

Fig. 14.
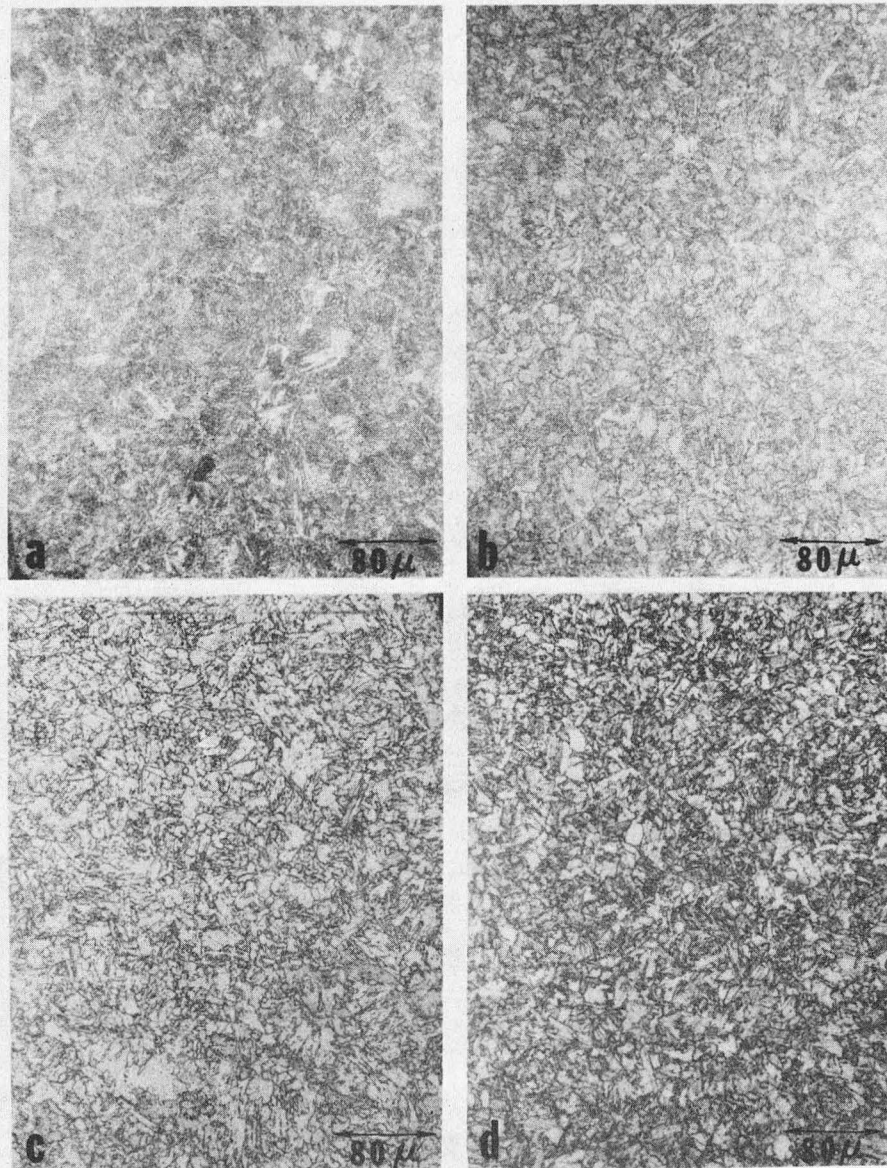
a : 800 °C
b : 800 °C & 600 °C
c : 800 °C, 710 °C & 600 °C
d : 800 °C, 670 °C & 600 °C
(1 hr / WQ)

XBB 806-7275

Fig. 15.
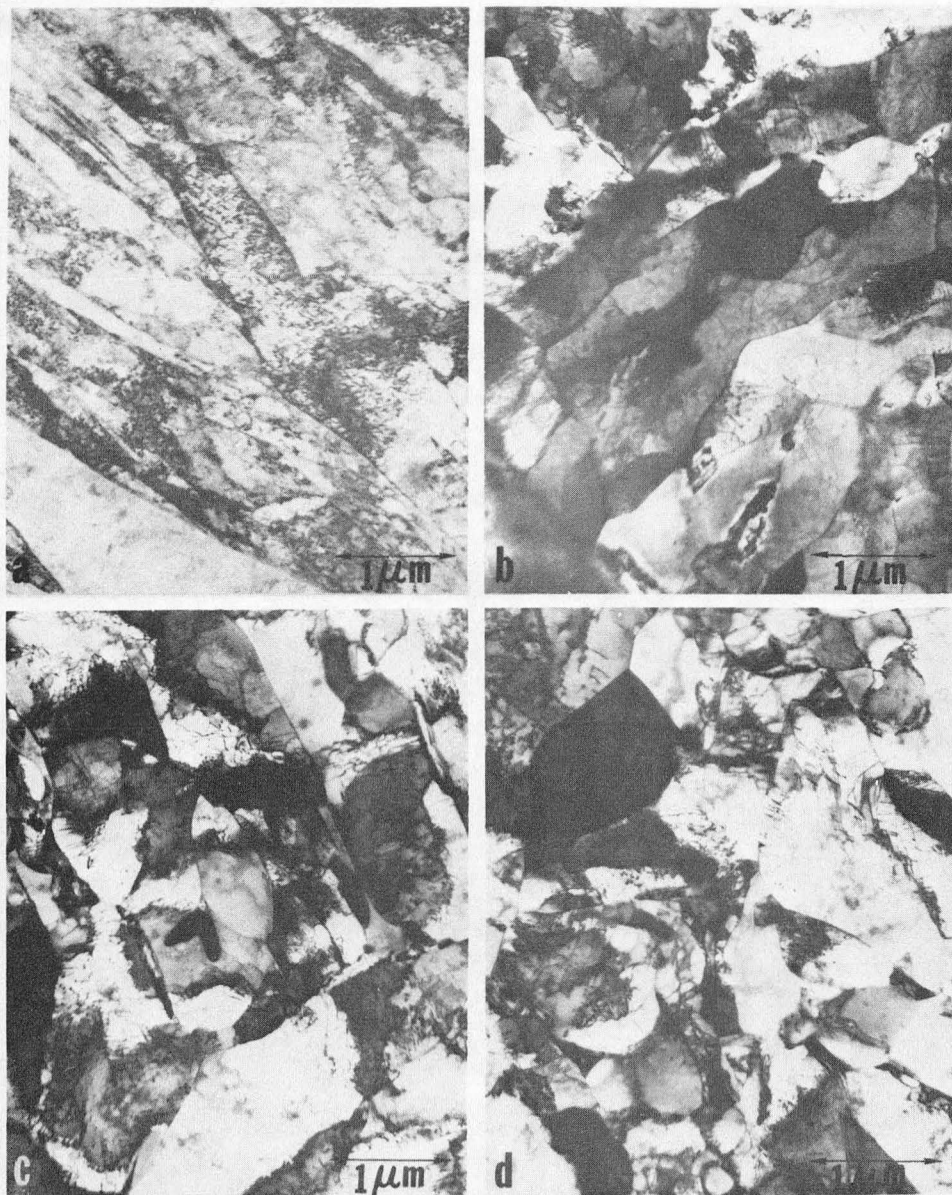
a : 800°C
b : 800°C & 600°C
c : 800°C, 710°C & 600°C
d : 800°C, 670°C & 600°C
(1 hr / WQ)

XBB 806-7276

Fig. 16.

R.T.

a; Q
b; QT
c; QL'T
d; QLT

Q; 800°C
L'; 710°C
L; 670°C
T; 600°C

I hr
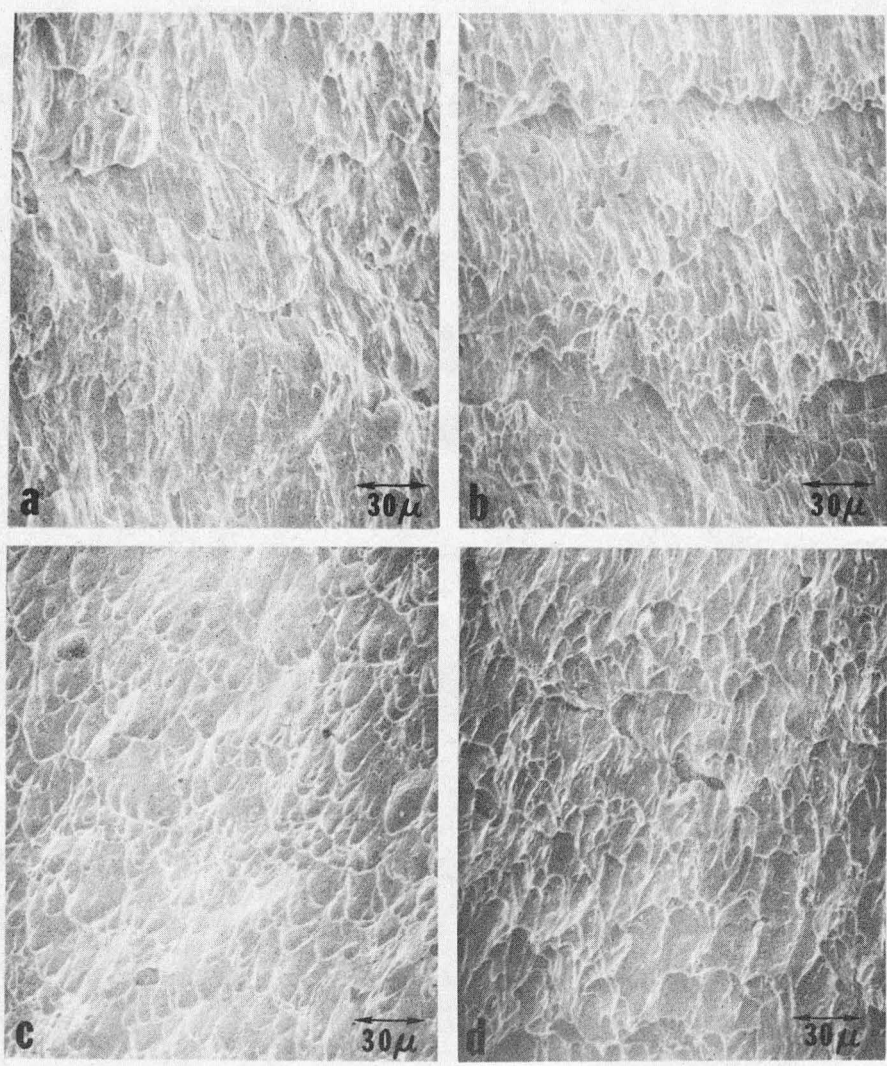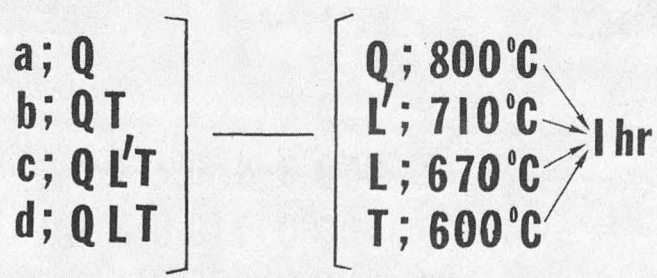
Fig. 17.
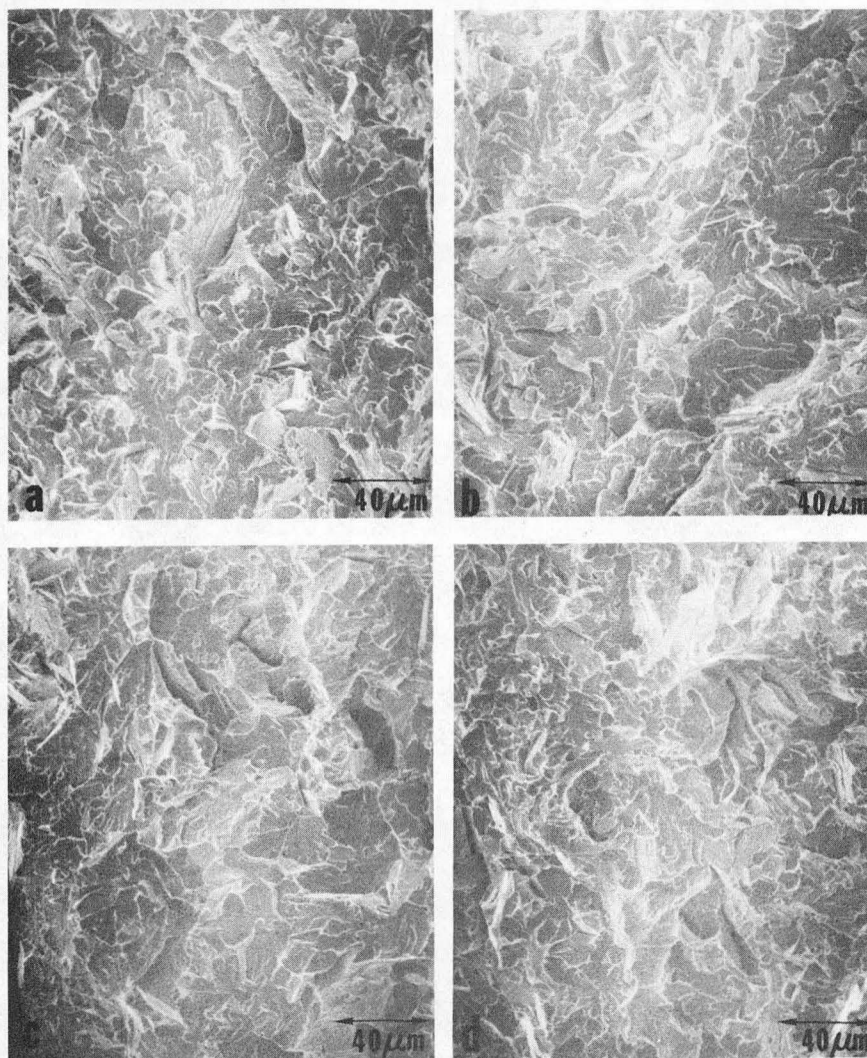
L.N.T.

a; Q
b; QT
c; Q L'T
d; Q LT

Q; 800°C
L'; 710°C
L; 670°C
T; 600°C
} 1 hr

XBB 806-7548

Fig. 18.
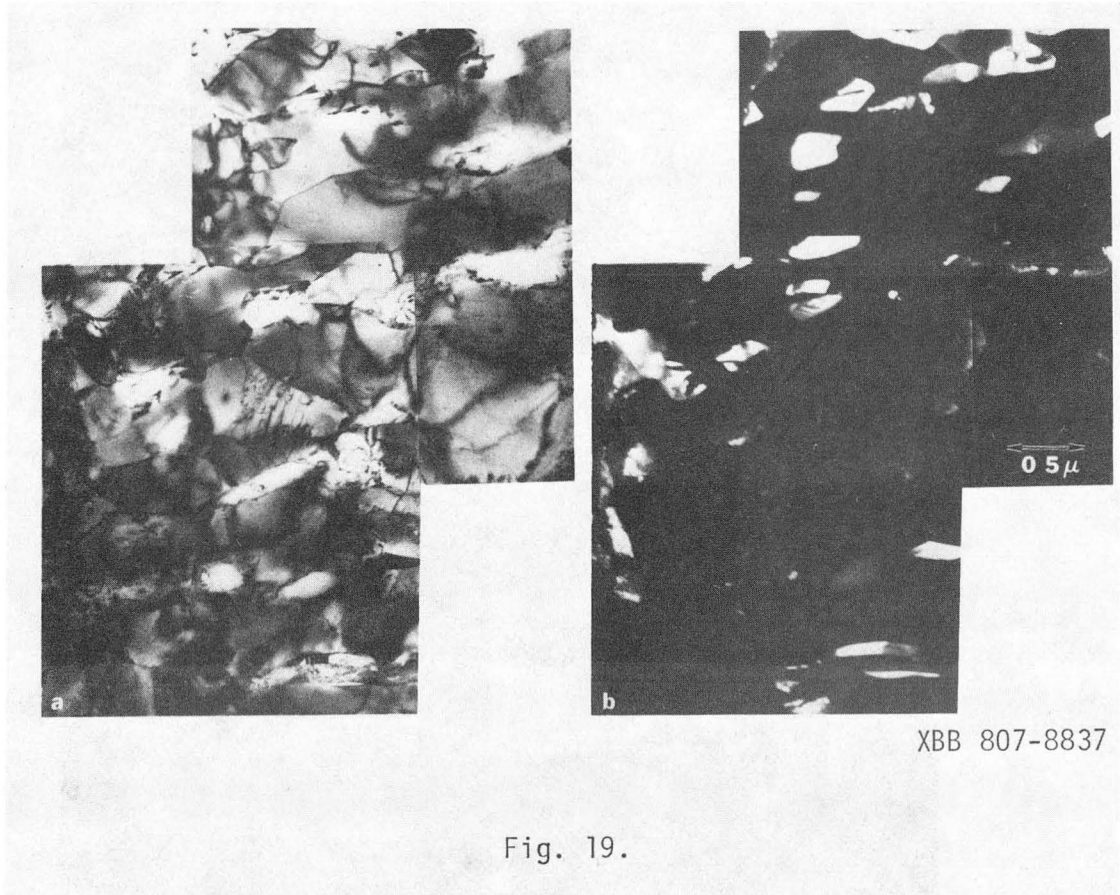
Fig. 19.
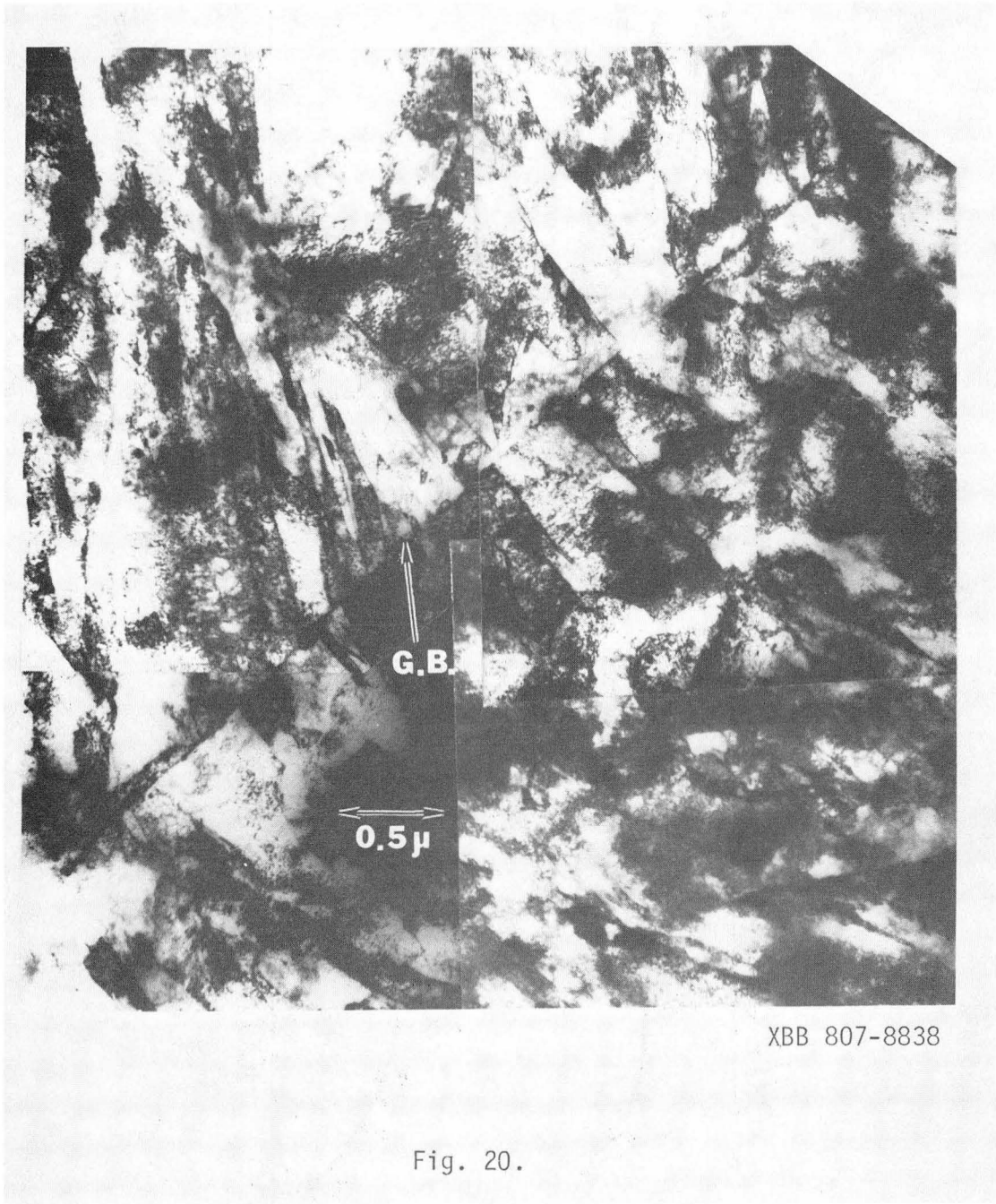
XBB 807-8837

XBB 807-8838

Fig. 20.
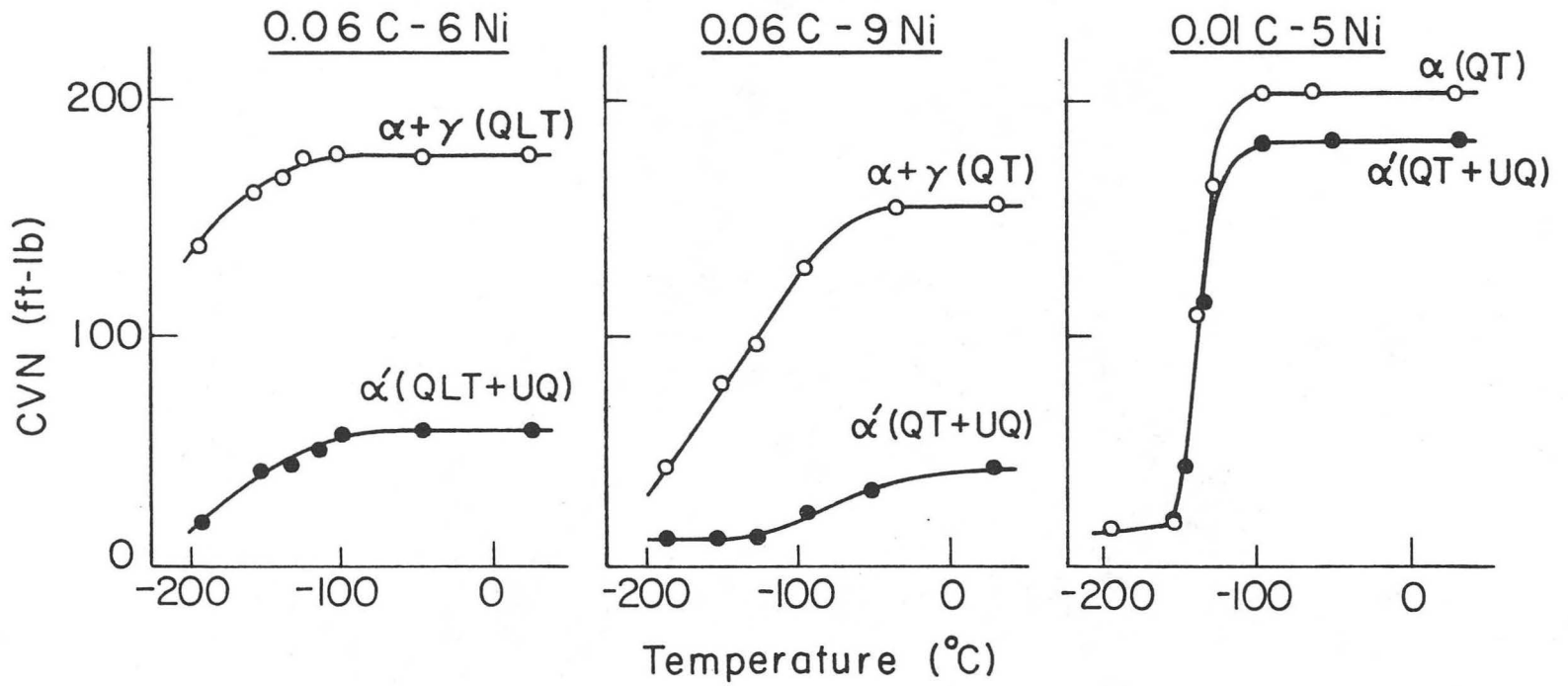
Fig. 21.

XBL 8012-13467
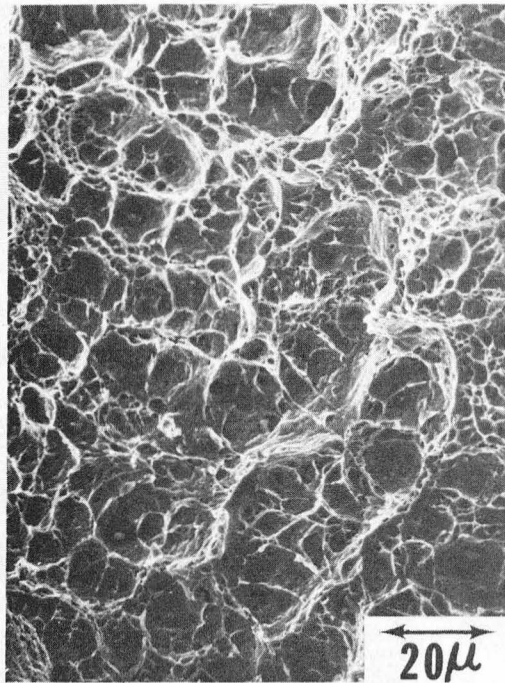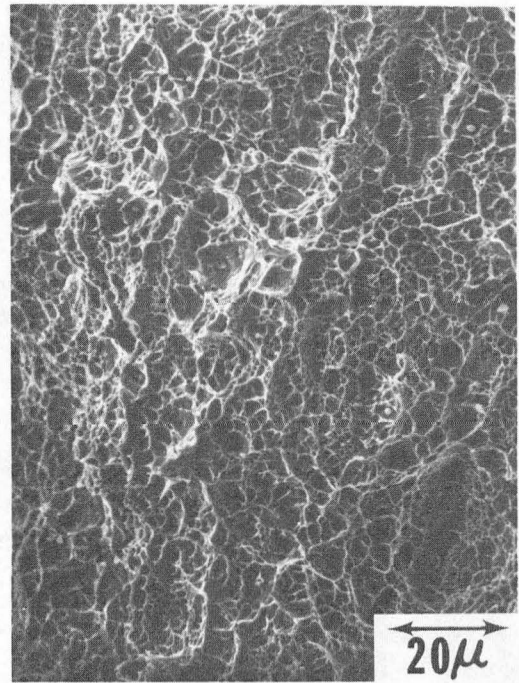
QT   QT+UQ

(R T)

XBB 807-8555

Fig. 22.
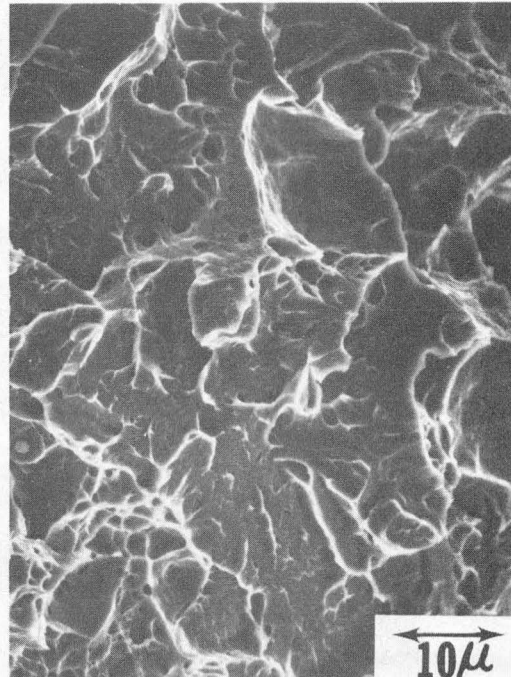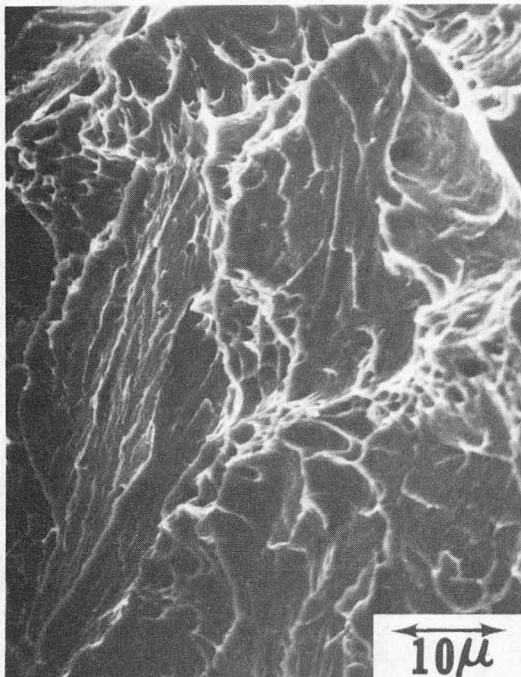
QT   QT+UQ

(LNT)

XBB 807-8554

Fig. 23.
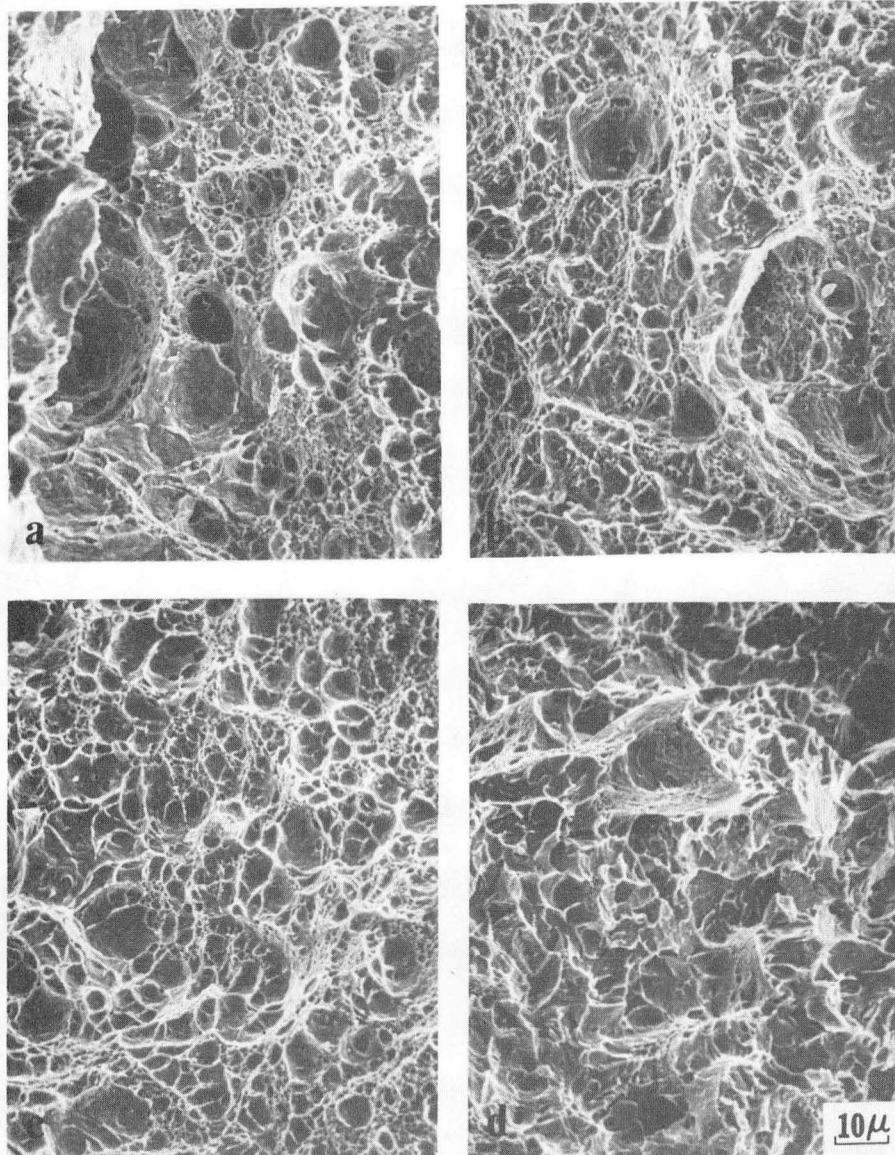
a;QLT(RT)   b;QLT(LNT)
c;UQ(RT)   d;UQ(LNT)

Fig. 24.